On Microscopic Traffic Models, Intersections and Fundamental Diagrams

by

Geoffrey McGregor
B.Sc., University of Victoria, 2011

A Thesis Submitted in Partial Fulfillment of the
Requirements for the Degree of

MASTER OF SCIENCE

in the Department of Mathematics and Statistics

On Microscopic Traffic Models, Intersections and Fundamental Diagrams

by

Geoffrey McGregor
B.Sc., University of Victoria, 2011

Supervisory Committee

Dr. R. Illner, Supervisor
(Department of Mathematics and Statistics)

Dr. M. Agueh, Member
(Department of Mathematics and Statistics)

Supervisory Committee

Dr. R. Illner, Supervisor
(Department of Mathematics and Statistics)

Dr. M. Agueh, Member
(Department of Mathematics and Statistics)

ABSTRACT

We design an Ordinary Delay Differential Equation model for car to car interaction with switching between four distinct force terms including "free acceleration", "follow acceleration", "follow braking", and "aggressive driving". We calibrate this model by recreating a real experiment on spontaneous formation of traffic jams. Once simulations of our model match those of the experiment we develop a model of both intersections using traffic lights, and intersections using roundabouts. Using our calibrated car interaction model we compare traffic light versus roundabout efficiencies in both flux and fuel consumption. We also use simulation results to extract information relevant to macroscopic traffic models. A relationship between flux and density known as The Fundamental Diagram is derived, and we discuss a technique for comparing microscopic to macroscopic models.

Contents

List of Figures

Chapter 1

Introduction

The study and analysis of vehicular traffic is motivated by the pursuit of improved safety and efficiency on our roadways. Such analysis of traffic breaks down into three main sections: Traffic modelling, optimization and traffic control. For a given problem, say, jam formation at a merging of two roads, each of these three sections plays a part in solving the problem. First, a mathematical model is needed which accurately represent how traffic flows, and how drivers interact with the particular section of road being studied. The optimization step, given some set of constraints, uses the mathematical model to compute an optimal solution, or best case scenario. Finally, using the mathematical model, the traffic control step studies what physical changes can be made to the road to ensure the optimal solution is more likely to occur. It is clear that success of this process hinges on the mathematical model's ability to accurately predict key features of real traffic flow. These features can be as simple as ensuring your model properly predicts jam formation and stop-and-go waves, or, as complex as when a car will change lanes, proceed through a yellow light, or merge into a roundabout. Throughout this thesis we develop a microscopic traffic model to be used in a detailed analysis of intersections, with an emphasis on how cars interact with roundabouts and traffic lights. This analysis gives us insight into which intersection types will be better at different densities, as well as specific traffic light timings and roundabout sizes to maximize flux and fuel efficiency.

When modelling traffic on a large scale, such as long stretches of highway, the use of microscopic models can be expensive computationally. This can be overcome in two ways, either a drastically simplified microscopic model is used, such as a cellular automata model, or by macroscopic modelling. Macroscopic models have proven to be an efficient way to tackle these large scale problems, however, frequently

their accuracy goes unchecked. These models are often benchmarked on their ability to predict traffic phenomena such as jam formation at bottlenecks, or stop-and-go waves, but the comparison to real traffic data is often overlooked. To overcome this we describe a technique for comparing microscopic models to macroscopic models as another way of checking the validity of macroscopic traffic predictions.

The majority of traffic modelling and simulation has been done through the use of microscopic or macroscopic traffic models. Microscopic models usually belong to one of two categories, either follow-the-leader type models or cellular automata models. Follow-the-leader models use the theory of ordinary differential equations to describe the position, velocity, and acceleration of vehicles. The first of these models was proposed by Pipes [5] with the simple assumption that cars accelerate linearly based on the difference in velocities between the following and leading cars, as in (1.1).

$$\dot{u}_{n+1}(t + \Delta t) = \lambda(u_{n+1}(t) - u_n(t)), \;\; \lambda \in \mathbb{R} \tag{1.1}$$

The obvious flaw of this model is the lack of speed limit, or desired speed for traffic to flow at. This drawback was addressed, and his ideas extended by many including Burnham [7] and Tyler [6] to list a couple. The study of follow-the-leader models has continued to progress with many notable contributions by Kerner [11] through the study of microscopic traffic flow with phase transitions. These phase transition microscopic models are highly complex and include a large number of parameters, some of which vary depending on the density.

Most other microscopic models are cellular automata models. These are discrete time models which use a simple set of rules to dictate change in car position and velocity. The roadway is split into cells, each of which is empty or contains a single car. A vehicle's velocity dictates how many cells it advances in each time step, and the acceleration varies depending on the chosen model. Among the first to study such models were Nagel and Schreckenberg in [10]. Their model consisted of the following four consecutive steps done at each time step:

1. **Acceleration**: if velocity v of a vehicle is lower than v_{max} and if the distance to the next car ahead is larger than $v + 1$, the speed advances by one ($v \to v + 1$).

2. **Slowing down (due to other cars)**: if a vehicle at sight i sees the next vehicle at sight $i + j$ (with $j \leq v$), it reduces its speed to $j - 1$, ($v \to j - 1$).

3. **Randomization**: With probability p, the velocity of each vehicle, (if greater

than zero), is reduced by 1 ($v \to v - 1$).

4. **Car motion**: each vehicle advances v sites.

Although this model is extremely simple, it does capture some important traffic phenomena such as traffic jam formation and stop-and-go waves. These models are very inexpensive to simulate and can handle millions of cars at once, not something easily done in a follow the leader type model. The cellular automata's ability to simulate such large scales, with reasonable results, has made it an invaluable tool in the analysis and prediction of large scale traffic systems all over the world.

For large scale modelling, the alternative to the cellular automata is the use of macroscopic traffic models. There is a wide range of models to choose from, including the fairly simplistic first order model studied by Lighthill and Whitham [3] and independently by Richards [4], the second order models studied by Aw and Rascle [1], and the non-local models studied by Illner and Herty [8, 9]. Many macroscopic models, including some mentioned here, assume a relationship between density and flux known as the fundamental diagram. Often, these fundamental diagrams are taken as functions relating each traffic density to a unique traffic flux. The validity of such a function is constantly under debate by researchers, with the massive amount of scattering observed in real traffic data, such as in Figure 1.1, being used as evidence against the existence of such fundamental diagrams. Using our microscopic traffic model we compute a fundamental diagram through simulation results. The resulting diagram matches observed trends in traffic, but also possesses the scattering seen in traffic data. We also show that a single fundamental diagram cannot work for all types of traffic, for example, a fundamental diagram for slow moving traffic in a city will not be the same as one for freeway traffic.

Dating back to the 1950's, the majority of traffic models, including most of these mentioned here, were focused on modelling and understanding highway traffic. This goal puts an emphasis on computational efficiency and models which focus on basic decision making by drivers. This leaves few options, if any, for small scale, high accuracy models needed in the analysis of specific traffic scenarios such as intersections with traffic lights, or roundabouts. To this end, we develop a follow-the-leader type model with discontinuous switches between four distinct force terms, including, "free acceleration", "follow acceleration", "following braking" and "aggressive driving". These force terms are not built to exaggerate certain traffic phenomenon, but instead are designed to capture how drivers actually interact with one another on the

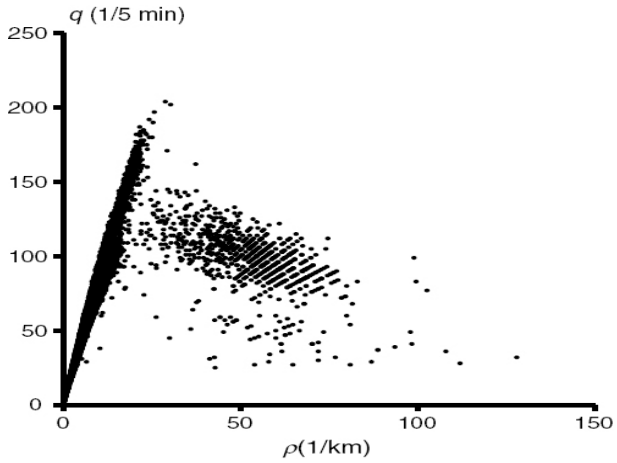

Figure 1.1: Data of traffic flux versus traffic density taken from [12].

road.

We begin Chapter 2 with a basic follow-the-leader model containing two forces, "follow acceleration" and "follow braking". The conditions for switching between these two forces is described, and we discuss the characteristics of the chosen force terms. From here, we introduce two additional force terms which we refer to as "free acceleration" and "aggressive driving", along with their respective switching conditions. With the inclusion of these terms we complete the microscopic model describing how cars interact with each other on the road, which we refer to as the Car Interaction Model. We then describe the numerical analysis of the model, insuring the numerical scheme accurately captures the discontinuities caused by the switching between force terms. The model is then calibrated to match video data in [12], used in the study of the spontaneous formation of traffic jams.

Chapter 3 is devoted to the modelling and analysis of different intersection types. We first describe how cars interact with traffic lights, including specifics to the three phases: Green, yellow and red. Also, we derive the additional force term, "Leader Brake", used by leading vehicles needing to stop at the intersection during a yellow or red light. Next, we take a similar approach to the modelling of roundabouts. We discuss in detail how cars use roundabouts, with an emphasis the merging process requiring the additional force term ,"Reduce Speed". To conclude this chapter we make comparisons between roundabouts and traffic lights in both fuel efficiency, and flux.

In Chapter 4 we switch gears and begin discussing macroscopic traffic models.

We discuss the relevance of the fundamental diagram to macroscopic modelling, and compute our own through simulation results. We also investigate the relationship between density and fuel consumptions in pursuit of a fuel consumption fundamental diagram.

In Chapter 5 we discuss key results as well as some directions for future research.

Chapter 2

Model Development and Calibration

2.1 The Car Interaction Model

We begin with a simple differential delay follow-the-leader model. This model attempts to capture the dynamics seen by cars driving on an open stretch of road. There is a leading car indexed by $i = 1$ and following cars, $i > 1$, which brake or accelerate depending on how their velocity relates to the car in front of them. Let $x_i(t)$ and $u_i(t)$ denote the position and velocity respectively of car i at time t. Using a constant reaction time $\tau > 0$, the conditions for switching between accelerating and decelerating are

$$\text{Condition 1: } u_{i-1}(t-\tau) - u_i(t-\tau) > 0$$
$$\text{Condition 2: } u_{i-1}(t-\tau) - u_i(t-\tau) \leq 0.$$

Car i will satisfy condition 1 if it's leading vehicle, car i-1, is traveling at a higher speed then car i. Since cars simply follow their leading car, car i will accelerate to match the velocity of car $i-1$. Condition 2 has car i-1 driving more slowly then car i. Here, car i will decelerate to match the velocity of car $i-1$. The constants required to model this basic two force model are described below. The constants in the above model are

- τ : Individual reaction time

- c_0 : Free acceleration constant
- c_1 : Follow acceleration constant
- k_1 : Follow braking constant
- L : Car length
- H : Minimum comfort distance
- u_{max} : Speed limit.

The parameters are self-explanatory with the exception of H, the minimum safety distance. This term describes the minimum distance a driver would want to have between them and their leading car. H is usually taken $\approx$ 2 meters, but in our case we measure distance as being front bumper to front bumper, therefore we take $H = L+2$. With the conditions for switching and the required parameters we suggest the two force follow-the-leader model.

$$\dot{x}_i = u_i \tag{2.1}$$

$$\dot{u}_i = \begin{cases} c_0 \cdot (u_{max} - u_i(t-\tau)) & \text{if } i = 1 \\ c_1 \cdot \left(\frac{1}{L} - \frac{1}{x_{i-1}(t-\tau) - x_i(t-\tau)}\right) \cdot (u_{i-1}(t-\tau) - u_i(t-\tau)) & \text{if 1 and } i > 1 \\ k_1 \cdot \left(\frac{1}{max(x_{i-1}(t-\tau) - x_i(t-\tau), H)}\right) \cdot (u_{i-1}(t-\tau) - u_i(t-\tau)) & \text{if 2 and } i > 1, \end{cases}$$

where 1 and 2 denote car i driving as in Condition 1 or 2 respectively. When a car with $i > 1$ encounters Condition 1, or "follow acceleration", we use the factor $\left(\frac{1}{L} - \frac{1}{x_{i-1}(t-\tau) - x_i(t-\tau)}\right)$. This can also be thought of as $(\rho_{max} - \rho(t-\tau))$ where ρ_{max} denotes maximum density, applying in bumper to bumper traffic, and $\rho(t)$ is the local density at time t. In the acceleration term it is important that the density portion be $\left(\frac{1}{L} - \frac{1}{x_{i-1}(t-\tau) - x_i(t-\tau)}\right)$ instead of $\left(\frac{1}{H} - \frac{1}{x_{i-1}(t-\tau) - x_i(t-\tau)}\right)$. One reason for this choice being that when traffic is bumper to bumper, $x_{i-1}(t-\tau) - x_i(t-\tau) = L$, we should have the density portion of the force term being zero, which is not satisfied by $\left(\frac{1}{H} - \frac{1}{x_{i-1}(t-\tau) - x_i(t-\tau)}\right)$. Another choice for the "follow acceleration" force would be $\left(\frac{1}{L} - \frac{1}{x_{i-1}(t-\tau) - x_i(t-\tau)}\right)^2$. The main issue with this choice is that it overemphasizes the density dependence of the acceleration term. When observing a platoon of cars accelerating from rest through a green light, drivers don't wait for large gaps to form

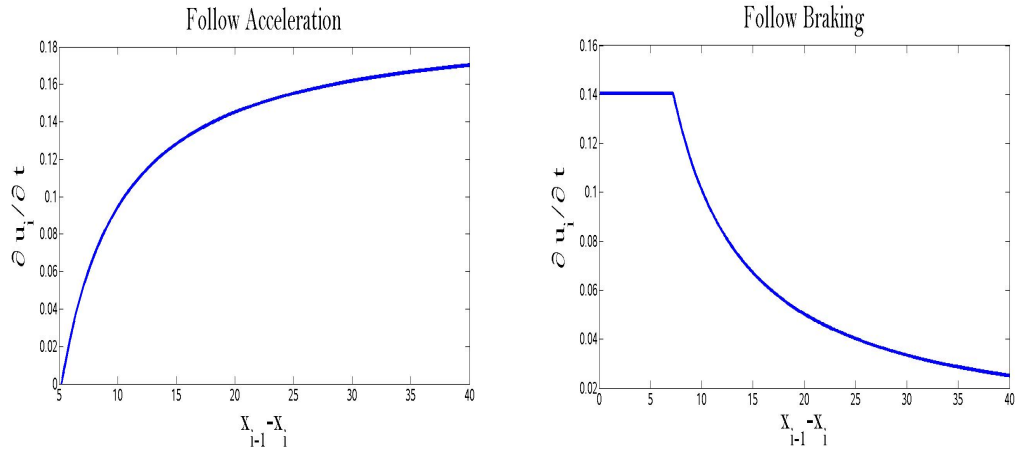

Figure 2.1: "follow acceleration" and "follow braking" plotted as a function of distance, $x_{i-1}(t-\tau) - x_i(t-\tau)$.

between themselves before accelerating, instead, they accelerate with the car in front of them. By squaring the density term it forces these large gaps to open before cars pick up speed, which is not realistic. In Figure 2.1 we have our chosen "follow acceleration" and "follow braking" terms plotted as a function of distance between cars, $x_{i-1}(t) - x_i(t)$, with $u_{i-1}(t-\tau) - u_i(t-\tau) = 1$.

The "follow braking" force includes $\left(\frac{1}{max(x_{i-1}(t-\tau)-x_i(t-\tau),H)}\right)$, a factor meant to capture the limitations on a vehicle's ability to brake, see Figure 2.1. There are many other possible choices, for example $\left(\frac{1}{\rho} - \frac{1}{\rho_{max}}\right)^{-1}$. This term has a similar slope to our choice, however, it does not capture braking limitations; in fact, it allows for an arbitrarily large braking force, seen in Figure 2.2, which is quite unrealistic.

In both following terms we multiply this density dependence term with a difference in velocity term. This term is reasonable, as the follower's will adapt to their leaders speed. This is a solid foundation for a car interaction model, however, some things need to be added to make it realistic. To start with, we need it to be possible for leaders to become followers and vise versa.

Definition 1 (Following Horizon)**.**
Let $i > 1$. Let D' denote some minimum viewing distance and let $T' \cdot u_i(t-\tau)$ denote a speed dependent viewing distance, which is, where car i will be in T' seconds if the speed $u_i(t-\tau)$ is sustained. If $x_{i-1}(t-\tau) - x_i(t-\tau) > max(D', T' \cdot u_i(t-\tau) + H)$ then car i drives as a leader, otherwise car i is a follower. We call $max(D', T' \cdot u_i(t-\tau) + H)$ the Following Horizon.

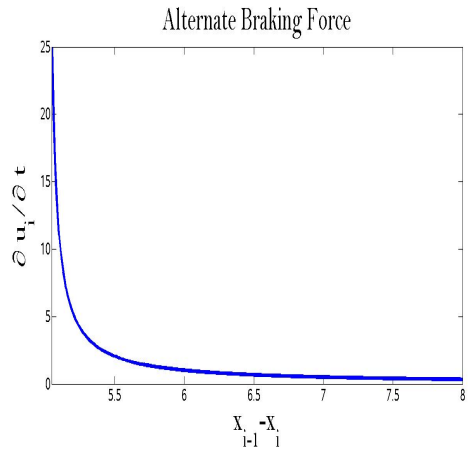

Figure 2.2: An alternate braking force.

Consider the following scenario. Assume car 1 is waiting at a stop light and car 2 is sitting at rest 20 meters behind. Now assume car 2 has car 1 in its following horizon, meaning $20 < max(D', T' \cdot u_2(t-\tau) + H)$, and is therefore "following" car 1. If we use the current model, (2.1), car 2 applies the "following braking" term, and since $u_{i-1} = u_i$ we have car 2 remain at rest. This is not a realistic reaction. In reality, car 2 would gradually accelerate and then come to a stop behind car 1 at the stop light. We capture this behaviour in the final term which we call "aggressive driving". We start by defining the needed parameters used in the new term.

- c_2 : Aggressive acceleration constant
- c_4 : Aggressive driving constant
- $\widetilde{T}$: 2 second rule

Similar to c_1, the constant c_2 scales the aggressive driving force term. c_4 dictates how "aggressive" a driver is, with a further explanation below, and $\widetilde{T}$ represents a driver's desire to be 2 seconds behind their leading car. The conditions for car i to apply the "aggressive driving" force are given by,

Condition 3: $x_{i-1}(t-\tau) - x_i(t-\tau) < max(D', T' \cdot u_i(t-\tau) + H)$
Condition 4: $H + \widetilde{T} \cdot u_i(t-\tau) < c_4(x_{i-1}(t-\tau) - x_i(t-\tau))$.

Condition 3 is the following horizon described above. Condition 4 relates car i's driving speed to the amount of empty space in front of them. This condition captures the desire for cars to drive approximately 2 seconds behind the car in front of them, commonly known as the 2 second rule. Therefore, if car i is satisfying Condition 4, then they feel that there is too much space between them and car $i-1$. When both of these conditions are met car i will enter the "aggressive driving" regime given by,

Aggressive Driving:

$$\dot{x}_i = u_i$$
$$\dot{u}_i = c_2 \cdot \left(\frac{1}{L} - \frac{1}{x_{i-1}(t-\tau) - x_i(t-\tau)} \right) \cdot (u_{max} - u_i(t-\tau)) \quad \text{if 3 and 4 hold.}$$

We call c_4, from Condition 4, the aggressive driving constant because it dictates in which situations a driver ignores the speed of the leading car and accelerates towards a desired speed. $H + \widetilde{T} \cdot u_i(t-\tau)$ is the distance car i will travel in $\widetilde{T}$ seconds if they maintain $u_i(t-\tau)$, plus the minimum safety distance H. $c_4(x_{i-1}(t-\tau) - x_i(t-\tau))$ is a fraction of the distance between car $i-1$ and car i at time $(t-\tau)$. So, if $c_4 = 1$ this would require that in $\widetilde{T}$ seconds car i travels at most $(x_{i-1}(t-\tau) - x_i(t-\tau)) - H$ meters. Basically, if car i maintained its speed for $\widetilde{T}$ seconds, regardless of car $i-1$'s speed, they will not collide. To model aggressive drivers we give them a high c_4, and a defensive driver would be given a low c_4. We provide more details in the next section.

With the inclusion of the aggressive driving term we have the full car interaction model.

Condition 1: $x_{i-1}(t-\tau) - x_i(t-\tau) < max(D', T' \cdot u_i(t-\tau) + H)$
Condition 2: $H + \widetilde{T} \cdot u_i(t-\tau) < c_4(x_{i-1}(t-\tau) - x_i(t-\tau))$
Condition 3: $u_{i-1}(t-\tau) - u_i(t-\tau) > 0$
Condition 4: $u_{i-1}(t-\tau) - u_i(t-\tau) <= 0$

$$\dot{x}_i = u_i \tag{2.2}$$

$$\dot{u}_i = \begin{cases} c_0 \cdot (u_{max} - u_i(t-\tau)) & \text{if not 1} \\ c_2 \cdot \left(\frac{1}{L} - \frac{1}{x_{i-1}(t-\tau) - x_i(t-\tau)}\right) \cdot (u_{max} - u_1(t-\tau)) & \text{if 1 and 2} \\ c_1 \cdot \left(\frac{1}{L} - \frac{1}{x_{i-1}(t-\tau) - x_i(t-\tau)}\right) \cdot (u_{i-1}(t-\tau) - u_i(t-\tau)) & \text{if 1, 3 and not 2} \\ k_1 \cdot \left(\frac{1}{max(x_{i-1}(t-\tau) - x_i(t-\tau), H)}\right) \cdot (u_{i-1}(t-\tau) - u_i(t-\tau)) & \text{if 1, 4 and not 2} \end{cases}$$

We argue that these four terms capture the key features of traffic dynamics. Some microscopic traffic models, such as [11], include many more terms including optimal driving speeds depending on density, different reaction times depending on the situation and forced over-acceleration or over-braking. We feel these extra terms are not necessary to capture desired traffic phenomena, such as traffic jam formation at a bottleneck, or stop and go waves.

The next step is to develop a numerical scheme to solve this model as accurately and efficiently as possible. Once we have our optimal scheme, we are able to calibrate the model's parameters to match real dynamics seen in traffic.

2.2 Numerical Analysis

Before implementing any numerical scheme it is important to analyze the characteristics of the original system. Our traffic model is a coupled system of differential delay equations with discontinuous acceleration terms. There is a vast amount of literature involving numerics on systems of delay equations, as well as numerics on ordinary differential equations with jump discontinuities; however, significantly less theory exists for systems which have a delay that also have discontinuities. Such discontinuities in differential equations are usually dealt with by fitting hyperbolic tangents to the jump, thus smoothing it out and allowing for the usual numerical methods to do their work. What makes this approach possible is that the jump is known ahead of time, as in, the left and right limits at the discontinuity are already known. In our situation, these jumps are not known ahead of time since traffic conditions dictate driver reactions at each time step. We deal with this by exploiting the delay in our equations.

To simplify our notation let $X(t-\tau) \in \mathbb{R}^2$ with $X(t-\tau) = (x_{i-1}(t-\tau), x_i(t-\tau))$.

We can rewrite equation (2.2) as

$$\dot{x}_i = u_i$$
$$\dot{u}_i = \Psi(X(t-\tau), u_{i-1}(t-\tau), u_i(t-\tau)), \text{ where } \Psi \text{ switches as in equation (2.2).}$$

The most basic approach would be to use forward Euler on both equations to get

$$\dot{x}_i \approx \frac{x_i(t+\Delta t) - x_i(t)}{\Delta t},$$

yielding,

$$x_i(t+\Delta t) \approx x_i(t) + \Delta t \cdot u_i(t).$$

Similarly for the change in velocity term,

$$u_i(t+\Delta t) \approx u_i(t) + \Delta t \cdot \Psi(X(t-\tau), u_{i-1}(t-\tau), u_i(t-\tau)).$$

Although this method is a very rough approximation of the actual model it doesn't run into any technical issues with the delay or the switching of acceleration terms. We now derive a more accurate method which deals with these complications just as easily.

For now we ignore the change in position term, $\dot{x}_i$, and focus on the acceleration term $\dot{u}_i$. We start by partitioning the time dimension into an evenly spaced grid with each point Δt apart. We also set $\Delta t << \tau$ to give a better approximation of the derivative (and another reason which will become clear in a moment).
Suppose we are at time t with $0 < t - \tau < t$. This means $X(s), u_i(s), u_{i-1}(s)$ are all known for $0 \leq s < t$. How do we calculate $u_i(t+\Delta t)$? We start by integrating both sides of the acceleration equation.

$$\int_t^{t+\Delta t} \dot{u}_i = \int_t^{t+\Delta t} \Psi(X(s-\tau), u_{i-1}(s-\tau), u_i(s-\tau))ds.$$

This implies

$$u_i(t+\Delta t) = u_i(t) + \int_t^{t+\Delta t} \Psi(X(s-\tau), u_{i-1}(s-\tau), u_i(s-\tau))ds,$$

which is equivalent to

$$u_i(t+\Delta t) = u_i(t) + \int_{t-\tau}^{t-\tau+\Delta t} \Psi(X(s), u_{i-1}(s), u_i(s))ds.$$

Since we chose $\Delta t << \tau$ we know the value of $\int_{t-\tau}^{t-\tau+\Delta t} \Psi(X(s), u_{i-1}(s), u_i(s))ds$ at the endpoints which permits the use of some basic numerical integration. The trapezoidal rules tells us

$$\int_{t-\tau}^{t-\tau+\Delta t} \Psi(X(s), u_{i-1}(s), u_i(s))ds \approx$$
$$\frac{\Delta t}{2}\left(\Psi(X(t-\tau+\Delta t), u_{i-1}(t-\tau+\Delta t), u_i(t-\tau+\Delta t)) + \Psi(X(t-\tau), u_{i-1}(t-\tau), u_i(t-\tau))\right).$$

Therefore we approximate $u_i(t+\Delta t)$ as

$$u_i(t+\Delta t) = u_i(t) +$$
$$\frac{\Delta t}{2}\left(\Psi(X(t-\tau+\Delta t), u_{i-1}(t-\tau+\Delta t), u_i(t-\tau+\Delta t)) + \Psi(X(t-\tau), u_{i-1}(t-\tau), u_i(t-\tau))\right).$$

We apply the same approach for the change in position term to get

$$x_i(t+\Delta t) = x_i(t) + \frac{\Delta t}{2}\left(u_i(t-\tau+\Delta t) + u_i(t-\tau)\right).$$

Before we use this method to solve our system we need to make sure it isn't violating the assumption that drivers can only react to what they have seen. This appears in the model through the delay term, $t-\tau$, and it is important that the model we obtain through this discretization maintains the same characteristics. First we discuss why it is beneficial to use an implicit type scheme when dealing with discontinuities.

Throughout this discussion we will frequently reference Figures 2.3 and 2.4 so we take a moment to ensure these plots make sense. In these figures we have plotted the driving conditions, $\Psi(X(t), u_{i-1}(t), u_i(t))$, as a function of time. It is important to notice that at each time t' car i won't react to the conditions $\Psi(X(t')), u_{i-1}(t'), u_i(t'))$ until time $t = t' + \tau$. Therefore each point $\Psi(X(t), u_{i-1}(t), u_i(t))$ is the force term car i will use at time $t+\tau$. Focusing on Figure 2.3, we wish to use our numerical scheme to approximate car i's response to their observed road conditions. At time t car i is referencing driving conditions at time $t-\tau$, which suggests braking. Notice at time t'

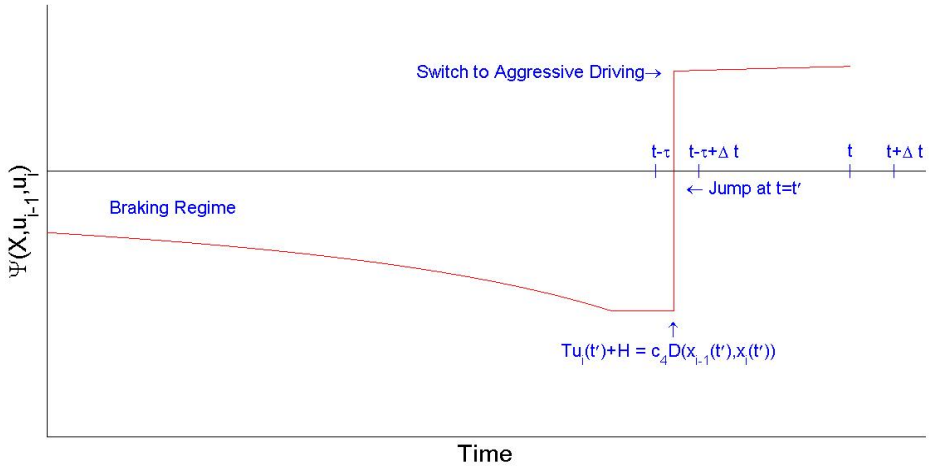

Figure 2.3: Sample Discontinuity in Acceleration

the driving conditions switch to an aggressive driving regime, which means car i wants to accelerate. In this case, we can see the exact conditions $\Psi(X(t), u_{i-1}(t), u_i(t)) \forall\, t \in [t-\tau, t-\tau+\Delta t]$, so we can calculate $u_i(t+\tau)$ as simply the area under the curve from time $(t-\tau)$ to $(t-\tau+\Delta t)$. In Figure 2.4 we see how the Euler method, on the left, compares to our trapezoidal method, on the right, with approximating the integral $\int_{t-\tau}^{t-\tau+\Delta t} \Psi(X(s), u_{i-1}(s), u_i(s))ds$.

It is immediately clear that the Euler method does a terrible job of catching the discontinuity in the acceleration. In fact, it says that car i should be braking hard for $\forall t \in [t, t+\Delta t]$, when in fact car i should brake $\forall\, t \in [t, t']$, and then accelerate $\forall \in t \in [t', t+\Delta t]$. This is not only a very poor approximation of the integral, but this error will change how car i+1 reacts, then how car i+2 reacts and so on. This could dramatically change the overall dynamics in a traffic simulation. On the other hand, we see the trapezoidal rule does a much better job of estimating the integral. This is because we are using information at both endpoints of the integrated region, but it raises the question whether or not we are violating the assumptions of the delay. The simple answer is no. Let's take a moment and forget about time being discretized and think about time flowing continuously. A driver at time t will be referencing time $(t-\tau)$ and will be continuously updating their information as time progresses. This means at time $(t+\epsilon)$ they are referencing $(t-\tau+\epsilon) \forall \epsilon \in \mathbb{R}^+$. Therefore their behaviour at $(t+\Delta t)$ is precisely determined by the conditions at

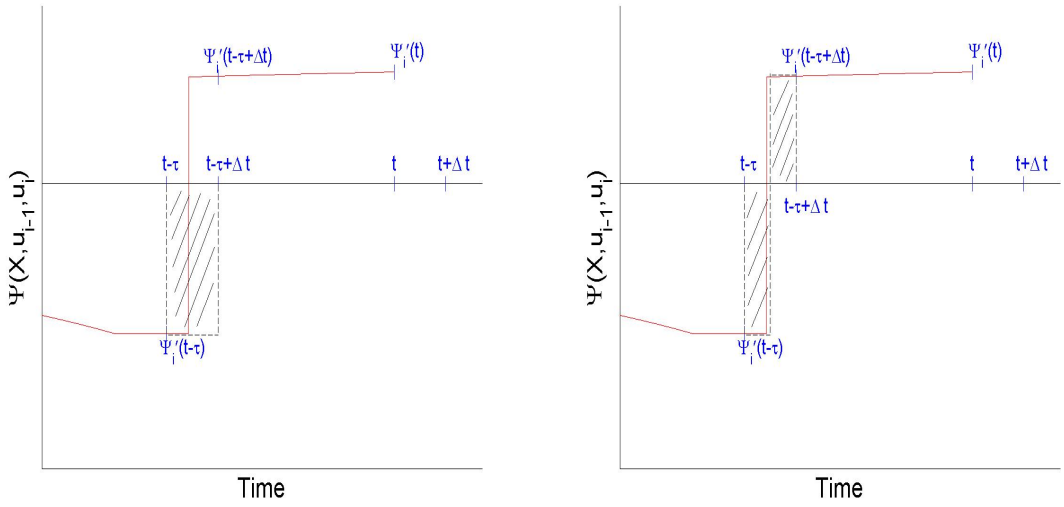

Figure 2.4: Two numerical methods are plotted, Euler on left and our trapezoidal rule on right

$(t - \tau + \Delta t)$. Our discretized model is estimating this continuous reference of (t) to $(t - \tau)$ through $(t + \Delta t)$ to $(t - \tau + \Delta t)$ and thus the use of the endpoint is not violating the assumption of a time delay.

2.3 Calibration of the Car Interaction Model

Now that we have the full car interaction model, we will choose the parameters to optimally represent real traffic flow. After numerous simulations we obtained reasonable estimates for the constants, c_0, c_1, c_2, c_4, k_1 and τ. The other constants, $D', T', \widetilde{T}$ and H were estimated from our own driving experience. To finalize the model we set up a simulation which matched a 2008 experiment done in Nagoya Japan, see [12]. The experiment was a 230 meter circular track with 22 cars where drivers were asked to drive along the track at 30 km/h for an extended period of time. What makes this experiment useful and relevant, is the spontaneous formation of traffic jams. We feel that if we recreate this experiment using our car interaction model and similar phenomenon appear, then we may have a realistic model for car to car interactions in moderate to high density traffic. Not only was the recreation of the Nagoya experiment used to justify the validity of the model, but it also was a great way to test the exact impact each constant had on the overall flow of traffic.

Here is a brief synopsis of the results.

2.3.1 Individual Reaction Time τ

The parameter τ has a massive impact on the overall flow of traffic. If τ is too big not only are crashes inevitable and frequent, but jams seem to appear too often, and their severity is unrealistic. If τ is too small traffic flows too efficiently. Jams will not appear without a serious perturbation, and once appeared, they will not persist. When τ is in a realistic range, all cars are able to react in time to smoothly come to a stop in almost all instances, however, even small perturbations in traffic can lead to traffic jams in certain density regimes. If τ is at the high end of this range, traffic is overly sensitive to perturbations and we don't get one large jam as seen in the experiment; instead, we see several small jams appear all over the circle, and the flow of traffic is very jerky. Conversely, if τ is at the bottom end of this range, as in people are able to react slightly too fast, jams become infrequent or non-existent at critical densities where jams are seen to form experimentally.

2.3.2 The Acceleration Constants c_1 and c_2

These constant dictates the rate of acceleration of a following car. When recreating the experiment studied in [12], we found that these constants can have a large impact on the persistence of traffic jams. If a car's acceleration is too gradual it creates a similar situation as seen by drivers taking too long to react to acceleration. This leads to the creation and persistence of jams. If cars are able to accelerate with the car in front of them then it is possible for traffic jams to reduce in size or disappear entirely. What we want to avoid is over acceleration leading to braking then back to accelerating and so on. This does happen in reality but only in certain situations, which are taken into account in the aggressive driving term.

2.3.3 Aggressive Driving Constant c_4

As mentioned above, a high c_4 is used to model aggressive driving and a low c_4 is for more defensive driving. Generally, drivers are comfortable driving about 2 seconds behind their leading car, with a minimum comfort distance of approximately 2 meters, hence, $\widetilde{T} = 2$ seconds, and $H = L + 2 \approx 7$ meters. With these in mind let us consider a defensive driver, say, with $c_4 = 1$, traveling at 15 m/s behind another vehicle where

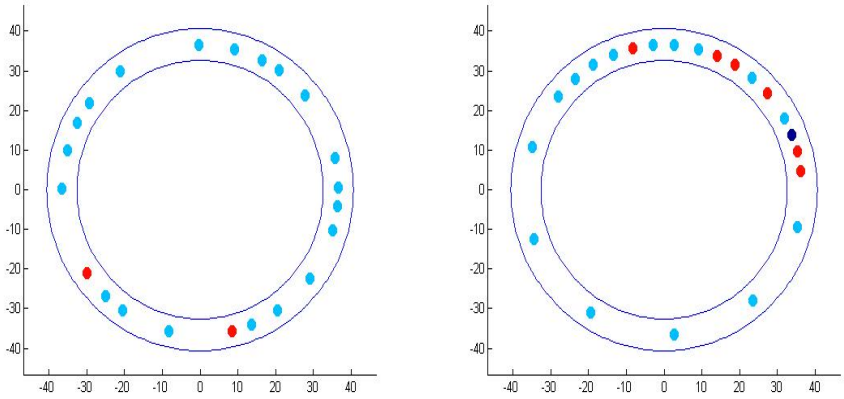

Figure 2.5: Unrealistic distributions of density in numerical circle experiment.

the speed limit is 20 m/s. Plugging in our numbers we get

$$H + \widetilde{T} \cdot u_i(t-\tau) = 7 + (2) \cdot (15) = 37.$$

Condition 2 from the car interaction model requires $H+\widetilde{T}\cdot u_i(t-\tau) < c_4(x_{i-1}(t-\tau)-x_i(t-\tau))$ for a car to enter the aggressive driving regime. Using the above calculation, Condition 2 is only satisfied if $37/c_4 < x_{i-1}(t-\tau) - x_i(t-\tau)$. This implies that our defensive driver, with $c_4 = 1$, will enter the aggressive driving regime if there is more than 37 meters between them and their leading car. In the same situation, but with a more aggressive driver, for example $c_4 = 4$, we have $37/c_4 = 9.25$ meters. This means that our aggressive driver would enter the aggressive driving regime as long as there was more than 9.25 meters between consecutive cars. This equates to driving $9.5 - L \approx 4.5$ meters from the rear bumper of the leading car. A behaviour commonly referred to as tailgating.

In our numerical tests we found that c_4 has a massive impact on the dynamics in the circle. In this experiment drivers were asked to drive 30 km/h throughout. This translates to some drivers not following the flow as much as trying to drive 30 km/h. This is not so different from a frustrated driver trying to get home quickly after work, behaviour exactly captured by the aggressive driving term! We found that to recreate the same dynamics as seen in the experiment we needed a higher c_4 than expected. This causes drivers to clump up, and results in more violent braking forces which, along with a reasonable choice of τ, causes traffic jams to form.

2.3.4 The "Follow Braking" Constant k_1

The braking constant is fairly self explanatory; it calibrates how hard cars will brake in a given situation. An obvious constraint on k_1 is that it has to be large enough such that, in almost all circumstances, cars are able to stop without crashing into one another. If k_1 is too large the force exerted on the driver would be highly unrealistic. This immediately gives a range of values for which the braking behaviour is plausible. When k_1 is at the upper end of this realistic range we think of it as modeling nervous drivers, braking is not smooth and often an overreaction to the situation. When running the numerical experiment with a large k_1, or nervous drivers, we consistently observed several small jams forming throughout the circle instead of cars clumping up in one spot. It is of course possible for several jams to form, although, this is not something that should happen in every simulation. We observed a similar phenomenon when we had τ too large. An example of this is seen in Figure 2.5.

2.3.5 Free Acceleration Constant c_0

Due to the number of cars in the circle each car's following horizon is non-empty and therefore the free acceleration term is not relevant in this experiment.

Chapter 3

Microscopic Modeling

3.1 Modeling Intersections with Traffic Lights

In this section we study a model of intersections using traffic lights with the car interaction model (2.2) as a base. The flow of traffic through an intersection is governed by the colour of the light, and the car to car interactions. This effectively breaks down into modeling traffic flow for the green, yellow and red stages of the traffic light. We will be concentrating on modeling a 4-way intersection with each incoming vehicle having the option of going straight, or making a right turn. In certain types of intersections, for example roundabouts, turning left is no different from going any other direction. This is not the case for intersections with traffic lights. With traffic lights, especially at high density, the majority of left turns happen during an advanced green light. This can allow both directions of traffic to turn left for a short time, or only give a green light to one direction of traffic. Sometimes the cars turning left get their own lane, sometimes they don't. To sum up, how left turns work at traffic lights depends heavily on the specific intersection. Including these different intersection setups would be very interesting and would certainly have an effect on intersection effectiveness. Looking into these specific intersections would make for an interesting case study but we will not do this here.

Consider the intersection to start at point -B and end at point B. Once a car is past point B, they only use the car interaction model since the rules of the light no longer effect them. See Figure 3.1. Before we are able to introduce how we modeled each phase of the traffic light, we need to add a force term which is not part of the car interaction model.

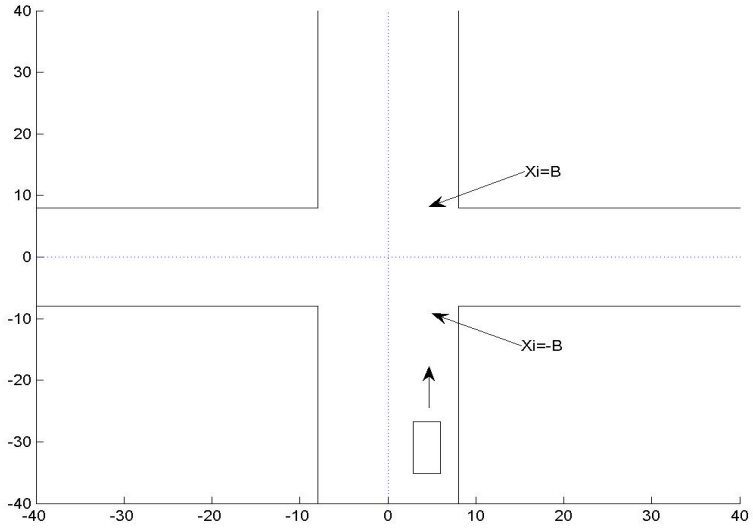

Figure 3.1: Sample intersection.

Suppose car i needs to come to a stop at point $-B$ with $x_i(t-\tau) < -B$ as shown in Figure 3.1. This is clearly not part of the car interaction model because this force is not a reaction to other vehicles on the road. We suggest the braking term

"Leader Brake":

$$\begin{aligned} \dot{x}_i &= u_i \\ \dot{u}_i &= k_0 \cdot \frac{1}{2|x_i(t-\tau) - (-B)|} \cdot u_i^2(t-\tau), \ k_0 < 0. \end{aligned} \tag{3.1}$$

This seems rather different from the terms in (2.2) but, in fact, arises from basic kinematics. We derive an equation relating velocity, distance and acceleration. The chain rule yields

$$\frac{d}{dt}\left(V^2(t)\right) = 2V(t)A(t), \ \text{ where V is velocity and A is acceleration.}$$

Integrating both sides from initial time, t_0, to final time, t_f, we get

$$V^2(t_f) - V^2(t_0) = 2\int_{t_0}^{t_f} V(t)A(t).$$

We want the braking force to be constant from t_0 until t_f, therefore we take $A(t)$ to be constant and using $\int_{t_i}^{t_f} V(t) = D$, the distance traveled, we get the equation

$$V_f^2 = V_0^2 + 2AD,$$

where V_f, V_0, A and D denote final and initial velocities, acceleration and distance respectively. Since car i wants to come to a stop at point $x = -B$ we have $V_0 = u_i(t_0 - \tau)$, $V_f = 0$ and $D = |x_i(t_0 - \tau) - (-B)|$. Solving for A we get

$$0 = u_i^2(t_0 - \tau) + 2A|x_i(t_0 - \tau) - (-B)|$$

therefore,

$$A = -\frac{u_i^2(t_0 - \tau)}{2|x_i(t_0 - \tau) - (-B)|}.$$

This choice of A will calculate the constant force required, given some initial speed $u_i(t_0 - \tau)$, to come to a stop at the desired intersection. This makes our force term

$$\dot{u}_i = k_0 \cdot \frac{1}{2|x_i(t - \tau) - (-B)|} \cdot u_i^2(t - \tau), \text{ with } k_0 \text{ a negative constant,}$$

as seen in (3.1). Notice that we do not include a maximum braking force as seen in the "follow braking" term. This is because drivers should not need to slam on the brakes when coming up to a stop light unless they weren't paying attention. This could be modeled separately but is not included in our simulations.

3.1.1 Green Light

Modeling driver behaviour in the green phase of a light is simple, all forces are dictated by (2.2).

3.1.2 Yellow Light

The yellow light phase breaks down into two parts: The moment the light turns from green to yellow, and the remaining portion of the yellow light. To properly model how traffic interacts with traffic lights we need to understand what is observed in reality. It turns out the initial reaction to the light change is the most important part.

Let us consider the moment when the light switches from green to yellow. Suppose that we have a steady flow of traffic through an intersection currently in the green

light phase. When the light switches to yellow there are several different things that happen depending on where the car is relative to the light.

1. The car is past the light so nothing changes because the light is no longer dictating that driver's behaviour.

2. The driver sees the light turn yellow, but decides he/she can safely pass through the intersection and does so.

3. The driver decides it is unsafe to follow the preceding car through the intersection and begins to brake.

4. The driver simply follows traffic flow which could include coming to a stop in a queue formed at the light, or the light is too far away to affect their driving.

To start, we define "too far away to affect the driver" to mean the intersection is not within the driver's following horizon. Assuming a driver is affected by the light, he/she will react to the transition from green to yellow by either following flow, or starting a braking trend. Once this initial choice is made, this behaviour will be retained throughout the rest of the yellow light phase. We model this mathematically as follows.

Suppose the light switches to yellow at time $t = t^*$ and stays yellow for T seconds. Drivers are able to react to the light switching τ seconds after it happens. Therefore, drivers don't notice that the switch has occurred until time $t^* + \tau$, at which time they perceive their position to be $x_i(t^* + \tau - \tau) = x_i(t^*)$. Let $\mathbb{S} = \{i | x_i(t^*) < -B\}$, the set of all cars which have not entered the intersection yet. Each car with i ϵ $\mathbb{S}$ computes $(T - \tau) \cdot u_i(t - \tau)$, where $(T - \tau) \cdot u_i(t - \tau)$ is how far the driver perceives they will travel in the remaining $(T - \tau)$ seconds of the yellow light. We now implement the four possible reactions to the yellow light, seen above, using our model and the values of $x_i(t - \tau)$ and $(T - \tau) \cdot u_i(t - \tau)$. Let $t = t^* + \tau$, and assume the same intersection setup as seen in Figure 3.1.

A. If the car j is already through the intersection then $j \notin \mathbb{S}$ and the driver is following the flow of traffic. This is modeled as follows,
If $j \notin \mathbb{S}$, then

$$\dot{x}_j = u_j$$
$$\dot{u}_j = \Psi(x, u), \quad \text{where } \Psi(x, u) \text{ is decided by (2.2).}$$

B. If car j sees the light switch and is close enough to the intersection to pass through, we have $j \in \mathbb{S}$ and $x_j(t-\tau) + (T-\tau) \cdot u_j(t-\tau) > B$. This is modeled as,
If $j \in \mathbb{S}$ and $x_j(t-\tau) + (T-\tau) \cdot u_j(t-\tau) > B$, then

$$\begin{aligned} \dot{x}_j &= u_j \\ \dot{u}_j &= \Psi(x,u), \quad \text{where } \Psi(x,u) \text{ is decided by (2.2).} \end{aligned}$$

C. If car j sees the light change and is too far away to follow car j-1 through the intersection we have $j \in \mathbb{S}$ and $x_j(t-\tau) + (T-\tau) \cdot u_j(t-\tau) < B$, so car j must come to a stop at the intersection. This is modeled by,
If $j \in \mathbb{S}$ and $x_j(t-\tau) + (T-\tau) \cdot u_j(t-\tau) < B$, then

$$\begin{aligned} \dot{x}_j &= u_j \\ \dot{u}_j &= k_0 \cdot \frac{1}{2|x_j(t-\tau) - (-B)|} \cdot u_j^2(t-\tau), \;\; k_0 < 0, \end{aligned}$$

which is the braking term (3.1).

D. If car j sees the light switch but it is rather too far away to worry about, or an earlier car began the braking trend we have $j \in \mathbb{S}$ and $((-B) - x_j(t-\tau)) < max(D', T' \cdot u_j(t-\tau) + H)$, or $x_{j-1}(t-\tau) + (T-\tau) \cdot u_{j-1}(t-\tau) < B$. This is modeled as,
If $j \in \mathbb{S}$ and $((-B) - x_j(t-\tau)) < max(D', T' \cdot u_j(t-\tau) + H)$, or $x_{j-1}(t-\tau) + (T-\tau) \cdot u_{j-1}(t-\tau)$, then

$$\begin{aligned} \dot{x}_j &= u_j \\ \dot{u}_j &= \Psi(x,u), \quad \text{where } \Psi(x,u) \text{ is decided by (2.2).} \end{aligned}$$

The yellow phase of a traffic light is by far the most complicated part of this type of intersection. To be used properly it requires drivers to have a clear perception of their speed, where they are relative to the intersection, how large the intersection is and also, what the other drivers are doing. Even with all of this complexity the main priority of drivers is to not crash into another vehicle, and this is why we need to use the car interaction model for all of the forces above except for the single vehicle which starts the braking trend.

3.1.3 Red Light

The red phase of the light has the basic property that no vehicles can pass through the intersection. In some places, right turns during the red phase are permitted, but we ignore them for now. This simplifies to the property that all cars must come to a stop at this light whether it be at the light, or behind another car. The difficulty is getting our model to do this in a realistic way.

Suppose there is a heavy stream of traffic going through an intersection governed by traffic lights. We have a good understanding of what happens to the flow once the light switches from green to yellow. A single car, say car j, will start a braking trend and the rest of the traffic will follow. In this case, when the light switches to red, cars will retain their behaviour from the yellow phase. Car j will come to a stop at the intersection and the subsequent cars continue to follow. To sum this up, if such a car j exists after the yellow light, then the red light phase is easy to model; however, there are instances where such a car j does not exist as the light switches to red. An example of this is when a car is approaching an intersection in the red phase, with no other vehicles between it and the intersection. This is uncommon in high density traffic, but must be included.

We model these ideas mathematically as follows. Let car i be traveling along a road towards a traffic light with $i-1 \notin \mathbb{S}$ as in Figure 3.1. Suppose the light switches from green to yellow at $t = t^*$ and from red to green at $t = t^* + t'$. Let $t\epsilon[t^*, t^* + t']$ with $i-1 \notin \mathbb{S}$ and $i \in \mathbb{S}$.
If $((-B) - x_i(t-\tau)) < max(D', T' \cdot u_i(t-\tau) + H)$

$$\begin{aligned} \dot{x}_i &= u_i \\ \dot{u}_i &= k_0 \cdot \frac{1}{2|x_i(t-\tau) - (-B)|} \cdot u_i^2(t-\tau), \quad k_0 < 0, \end{aligned}$$

otherwise,

$$\begin{aligned} \dot{x}_i &= u_i \\ \dot{u}_i &= \Psi(x,u), \quad \text{where } \Psi(x,u) \text{ is decided by (2.2).} \end{aligned}$$

3.2 Modeling Intersections with Roundabouts

In this section we study roundabouts. Unlike intersections governed by traffic lights, the efficiency of a roundabout is heavily dependent on the drivers using it. For example, when a car is coming up to a traffic light the decision of whether to proceed or brake is mostly dependent on the colour of the light. The only time a driver needs to make a decision is when the light switches to yellow, and he or she decides to stop or go. With roundabouts, each approaching driver needs to make a decision to stop at the yield line, or reduce their speed and merge. This is no simple decision: It depends not only on their speed and position relative to the yield line, but also on the positions and speeds of the cars within the roundabout. This extra dependence on the driver allows for a lot more variation in the effectiveness of the intersection. For example, in high density traffic an aggressive driver may merge allowing the incoming road to flow, whereas a defensive driver may have to wait a significant amount of time, potentially leading to the formation of a queue. Since we want to make direct comparisons between traffic lights and roundabouts, it is in our best interests to use our car interaction model (2.2) as much as possible. By doing this, it better simulates the same set of drivers used for all experiments.

Up to this point we have only used the car interaction model to capture dynamics of traffic along straight stretches of road. This meant the distance between vehicle i and vehicle j at time t was given by, $\mathcal{D}\big(x_i(t), x_j(t)\big) = |x_i(t) - x_j(t)|$, the 1-dimensional Euclidean distance. Since single lane roads are 1-dimensional curves, we are able to translate the curved roads into straight roads and then use the original car interaction model. One may argue that this is naive to assume that curved roads are driven the same as straight roads. This is a valid point, however , it is easy to implement a lower speed limit on the translated road to mimic the speed reduction required for sharp turns. We now look in detail at how the car interaction model works in a roundabout.

3.2.1 Implementation of the Car Interaction Model into a Roundabout

To keep things simple we will consider a 4-entrance and 4-exit roundabout as seen in Figure 3.2. In this section we frequently refer to roundabouts having some radius R. By this we mean cars traveling in the roundabout of radius R are at a distance R from the centre of the circle. To properly model roundabouts, we not only need our

car interaction model governing flow along the incoming and outgoing roads, but also inside the roundabout itself. This means we need to calculate distances between cars in a different way. As mentioned above, we do this by translating the curved road into a straight road, using the original model (2.2) to compute driver behaviour, then translating the results back to the curved road. This is illustrated in the following example.

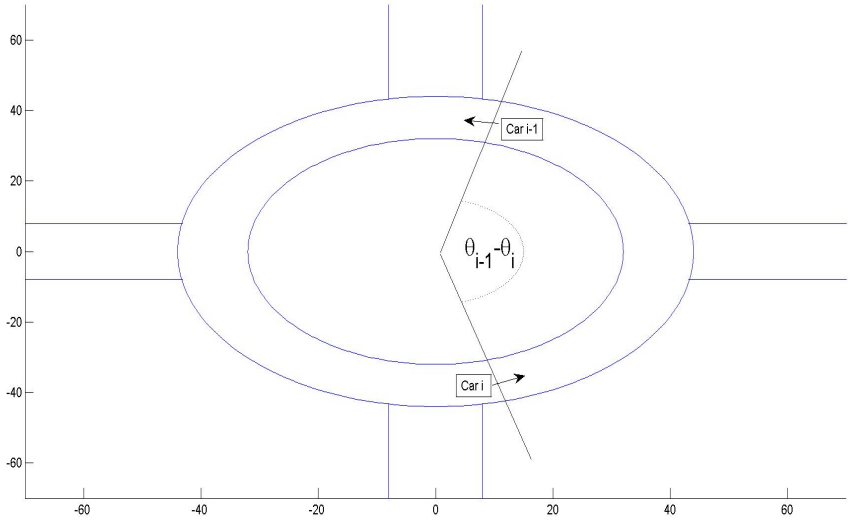

Figure 3.2: Sample 4-entrance 4-exit roundabout.

Consider two cars traveling in a roundabout of radius R with car i traveling behind car i-1 at perceived positions $x_i(t-\tau) = \big(w_i(t-\tau), y_i(t-\tau)\big) \in \mathbb{R}^2$ and $x_{i-1}(t-\tau) = \big(w_{i-1}(t-\tau), y_{i-1}(t-\tau)\big) \in \mathbb{R}^2$. We wish to compute $\mathcal{D}\big(x_{i-1}(t-\tau), x_i(t-\tau)\big) = \mathcal{D}\Big(\big(w_{i-1}(t-\tau), y_{i-1}(t-\tau)\big), \big(w_i(t-\tau), y_i(t-\tau)\big)\Big)$, the perceived distance between the two cars to allow the use of the car interaction model. In this situation we take $\mathcal{D}\big(x_{i-1}(t-\tau), x_i(t-\tau)\big)$ to be the arc length of the circle between the two cars. Using $\big(w_i(t-\tau), y_i(t-\tau)\big)$ and $\big(w_{i-1}(t-\tau), y_{i-1}(t-\tau)\big)$ along with basic trigonometry we compute their angles in the circle θ_{i-1} and θ_i, respectively. The angle between them is given by $(\theta_{i-1} - \theta_i) \mod 2\pi$, seen in Figure 3.2. Dividing this by 2π gives the percentage of the circle taken up by $(\theta_{i-1} - \theta_i) \mod 2\pi$. This fraction of 2π is translated into a distance through the equation

$$\mathcal{D}\big(x_{i-1}(t-\tau), x_i(t-\tau)\big) = 2\pi R \frac{(\theta_{i-1} - \theta_i) \mod 2\pi}{2\pi}, \tag{3.2}$$

which is the arc length between angles θ_{i-1} and θ_i. Therefore, cars traveling within the roundabout use the car interaction model (2.2) with $|x_{i-1}(t-\tau)-x_i(t-\tau)|$ given by (3.2). Now that we have modeled how traffic flows both inside, and outside the roundabout we need to model how cars merge into the roundabout. We cover this in the next section.

3.2.2 Merging into a Roundabout

When a car is approaching a roundabout there are several things that can happen. We list a few possible scenarios. Let U_c denote the speed limit within the roundabout.

1. The roundabout is empty so the driver reduces their speed to U_c and then merges into the roundabout.

2. The roundabout is full of cars so the driver comes to a stop at the yield line and waits for an opening before merging.

3. The roundabout is not empty and the driver has to reduce his or her speed to allow for an opening. Once the opening appears they speed back up to U_c and merge.

It may seem that scenarios 2 and 3 are quite similar, however, it is important to note that it is possible for cars to completely stop at the yield line as well as merge at a speed less than U_c. There are situations when the roundabout is not empty but the driver is able to merge at U_c, the same as in scenario 1. This is because drivers only survey a certain section of the roundabout to see whether or not it is safe to merge. We will call this section the merger window. If this merger window has no cars in it then the driver behaves as in scenario 1. If the merger window is not empty, as in scenario 3, then the driver must reduce his or her speed to allow the cars to pass out of their merger window. If the merger window remains not empty, as in scenario 2, then the driver must come to a full stop at the yield line. This merger window needs to shift depending on where the driver is relative to the merging point, and the size of the window should be dictated by how aggressive or defensive the driver is. We next capture these observations mathematically.

Let car i be traveling towards a roundabout with the centre of the circle being at $(0,0) \in \mathbb{R}^2$. The incoming road meets the roundabout at the yield line $\big(w,y\big) = \big(0,-B\big)$. Car i's perceived distance from the yield line is $|x_i(t-\tau)-(-B)| = D$

as seen in Figure 3.3. We define the point P, shown in Figure 3.3, as D meters of arc length from the merger point in the direction of oncoming traffic. Using polar coordinates and the entrance angle, which in the case of Figure 3.3 is $\frac{3\pi}{2}$, we compute the point P as

$$P = \left(R\cos\left(\frac{3\pi}{2} - 2\pi\frac{D}{2\pi R}\right), R\sin\left(\frac{3\pi}{2} - 2\pi\frac{D}{2\pi R}\right)\right), \text{ or,}$$

$$P = \left(R\cos\left(\frac{3\pi}{2} - \frac{D}{R}\right), R\sin\left(\frac{3\pi}{2} - \frac{D}{R}\right)\right).$$

Since point P will exist for all merging vehicles, not just ones coming from entrance angle $\frac{3\pi}{2}$, we define a general point P for cars merging from entrance angle ϕ.

$$P = \left(R\cos\left(\phi - \frac{D}{R}\right), R\sin\left(\phi - \frac{D}{R}\right)\right).$$

As mentioned above, when cars are traveling towards a roundabout they look at a particular section of the road to decide if they can merge or if they need to stop. We define this section of the road as "the merger window", an open interval centred at the point P. This interval can be a set of angles or a set of points; we use angles for now to simplify things. We want the merger window to change size depending on driver aggression, and current speed. To achieve this we start by defining a positive function $F(c_4, u_i(t-\tau)) \geq 1 \; \forall \; c_4, \; u_i(t-\tau) \in \mathbb{R}^+ \cup \{0\}$. This positive function F will determine the size of car i's merger window. We want F to be a decreasing function of both c_4 and $u_i(t-\tau)$ because a more aggressive driver will need a smaller gap in traffic to merge, and a slower moving car will require a larger gap in traffic. We define a merging window for car i with entrance angle ϕ as

$$MW_i(t) = \left\{ \theta \in [0, 2\pi) \,\middle|\, \theta \in \left(\phi - \frac{D}{R} - \frac{F_i(c_4, u_i(t-\tau)) \cdot H}{R}, \phi - \frac{D}{R} + \frac{F_i(c_4, u_i(t-\tau)) \cdot H}{R} \right) \right\}.$$

The set MW_i is illustrated in Figure 3.3.

There are many possible choices for the function F including the example seen in (3.3). In this case F does not depend on c_4, making it a good choice when all drivers have the same c_4. With this choice of F, driver's approaching the roundabout with $u_i(t-\tau) \geq U_c$ only survey $1.5 \cdot H$ meters to either side of point P, whereas driver's sitting at the yield line with $u_i(t-\tau) = 0$ survey $2.5 \cdot H$ meters to either side of point

P.

$$F = \min\left(1.5 \cdot H + H \cdot \max\left(\left(\frac{U_c - u_i(t-\tau)}{U_c}\right), 0\right), 2.5 \cdot H\right). \tag{3.3}$$

We say a car j at point (w_j, y_j) is in car i's merging window if car j's perceived angle $\theta_j = \cos^{-1}\left(\frac{w_i(t-\tau)}{R}\right) \cap \sin^{-1}\left(\frac{y_i(t-\tau)}{R}\right) \in MW_i(t)$. Cars will only begin looking at their merger windows once the yield line is within their following horizon.

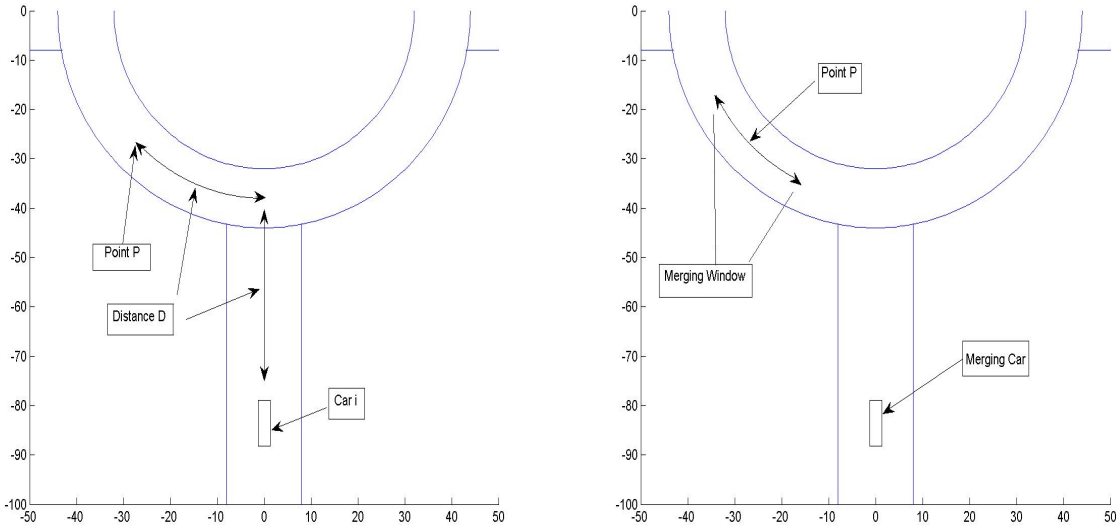

Figure 3.3: Merging window.

To fully model a roundabout we need an additional force term which allows for cars to slow down to U_c before merging. Assuming the merger window remains empty and $u_i(t_i - \tau) > U_c$ we want the deceleration to U_c from $u_i(t_i - \tau)$ to be constant. This allows the use of the same kinematic equation used to derive equation (3.1), except $V_f = U_c$ instead of $V_f = 0$. Therefore, when a car is approaching an empty roundabout with $u_i(t_i - \tau) > U_c$ they apply the force "Reduce Speed" given by

$$\begin{aligned} \dot{x}_i &= u_i \\ \dot{u}_i &= k_0 \cdot \frac{u_i^2(t-\tau) - U_c^2}{2|x_i(t-\tau) - (-B)|}, \quad k_0 < 0. \end{aligned} \tag{3.4}$$

This will apply constant deceleration to ensure when $x_i(t_f) = (-B)$ that we have $U_i(t_f) = U_c$. This force will be used by all merging vehicles whenever their merger window is empty and $u_i(t_i - \tau) > U_c$.

Currently a merging vehicle will either be using equation (3.1) if their merger window is non-empty, or equation (3.4) if $u_i(t_i - \tau) > U_c$ and their merger window is empty. It is possible for merging vehicles to have an empty merging window with $u_i(t_i - \tau) < U_c$, therefore, we need a term for accelerating towards U_c. Every vehicle that has been stopped at the entrance of the roundabout, or is approaching the roundabout with a reduced speed will use this acceleration term. If car i's merger window is empty and $u_i(t_i - \tau) < U_c$ they will accelerate up to U_c using the free acceleration force

$$\begin{aligned} \dot{x}_i &= u_i \\ \dot{u}_i &= c_0 \cdot (U_c - u_i(t - \tau)). \end{aligned} \tag{3.5}$$

With the inclusion of equation (3.5) we argue that we have all the force terms required to capture the dynamics seen in vehicles merging into roundabouts. Using these terms we add a few subtle details to the merging process.

If we stick with the current model for merging, it is possible for cars to repeatedly switch between an empty merger window and a non-empty merger window. This can occur by cars slowing down due to a non-empty merger window. This slowing can allow the merger window to become empty again, causing the car to accelerate towards U_c. This acceleration can result in the merger window becoming non-empty again. This process can continue until the merging vehicle is exactly distance R from the centre of the circle, at which point they follow the flow within the roundabout. Also, with the current model, the cars driving within the roundabout will ignore this slowly merging vehicle up until they reach that distance R. This is highly unrealistic because at some point the front of the merging car would cross the path of the flowing traffic, causing a collision. Again, this type of collision can occur; however, this type of scenario is not something we need to include in our model. To avoid this from occurring we need a point of no return for merging vehicles. This point will be a distance from the roundabout traveling radius, R, for which merging vehicles simply commit to merging and traffic reacts to this merging vehicle.

Definition 2 (Point of No Return)**.**
Let the centre of a roundabout be at $(0, 0) \in \mathbb{R}^2$ *with radius R. Suppose also that the yield line for this roundabout is distance B away from* $(0, 0)$*. Let car i be a merging vehicle approaching the yield line, therefore* $\sqrt{\big(w_i(t - \tau)\big)^2 + \big(y_i(t - \tau)\big)^2} > B$*. If at*

some time, say t', $R < \sqrt{\big(w_i(t'-\tau)\big)^2 + \big(y_i(t'-\tau)\big)^2} < R + L$, then car i switches to the roundabout free acceleration force (3.5) until merged. Cars in the roundabout which are approaching this merging point at time t' react to car i once they switch to force (3.5). The distance $R + L$ is referred to as the "point of no return".

With the inclusion of the point of no return we are able to fully model the interaction of a car and a roundabout.

Let car i be traveling towards a roundabout of radius R at the entrance angle ϕ with the yield line distance B from the centre of the circle. If the yield line is too far away to affect the behaviour of car i then they simply follow the flow of traffic. Therefore, If $|(-B) - x_i(t-\tau)| > max(D', T' \cdot u_i(t-\tau) + H)$ then

$$\begin{aligned} \dot{x}_i &= u_i \\ \dot{u}_i &= \Psi(x,u), \quad \text{where } \Psi(x,u) \text{ is decided by (2.2).} \end{aligned}$$

If the yield line is within the following horizon then car i begins to look at their merging window, as well as following traffic flow. If car i-1 hasn't merged yet then car i must follow the flow to prevent crashing. This is captured mathematically as,
if $|(-B) - x_i(t-\tau)| < max(D', T' \cdot u_i(t-\tau) + H)$ and $x_{i-1}(t-\tau) < -B$ then

$$\begin{aligned} \dot{x}_i &= u_i \\ \dot{u}_i &= \Psi(x,u), \quad \text{where } \Psi(x,u) \text{ is decided by (2.2).} \end{aligned}$$

If car i-1 has merged then car i looks at their merging window, if the window is empty then they accelerate or decelerate to match the roundabout speed U_c which is modeled as,
if $|(-B) - x_i(t-\tau)| < max(D', T' \cdot u_i(t-\tau) + H)$, $x_{i-1}(t-\tau) > -B$, $\big|MW_i(t)\big| = 0$ and $u_i(t-\tau) < U_c$ then

$$\begin{aligned} \dot{x}_i &= u_i \\ \dot{u}_i &= k_0 \cdot \frac{u_i^2(t-\tau) - U_c^2}{2|x_i(t-\tau) - (-B)|}, \quad k_0 < 0. \end{aligned}$$

If $|(-B) - x_i(t-\tau)| < max(D', T' \cdot u_i(t-\tau) + H)$, $x_{i-1}(t-\tau) > -B$, $\left|MW_i(t)\right| = 0$ and $u_i(t-\tau) \geq U_c$ then

$$\begin{aligned} \dot{x}_i &= u_i \\ \dot{u}_i &= c_0 \cdot (U_c - u_i(t-\tau)). \end{aligned}$$

If car i-1 has merged and car i's merger window is not empty then they come to a stop at the yield line. This is described mathematically as,
if $|(-B) - x_i(t-\tau)| < max(D', T' \cdot u_i(t-\tau) + H)$, $x_{i-1}(t-\tau) > -B$ and $\left|MW_i(t)\right| \neq 0$ then

$$\begin{aligned} \dot{x}_i &= u_i \\ \dot{u}_i &= k_0 \cdot \frac{1}{2|x_i(t-\tau) - (-B)|} \cdot u_i^2(t-\tau), \quad k_0 < 0. \end{aligned}$$

Lastly if they cross the point of no return they must commit to merging. This is modeled as,
if $R < \sqrt{\left(w_i(t'-\tau)\right)^2 + \left(y_i(t'-\tau)\right)^2} < R + L$ then

$$\begin{aligned} \dot{x}_i &= u_i \\ \dot{u}_i &= c_0 \cdot (U_c - u_i(t-\tau)). \end{aligned}$$

Once merged, cars follow the modified car interaction model with distance as in equation (3.2). When they exit onto their desired road, they return to the usual car interaction model (2.2).

Now that we have finished modeling both traffic light and roundabout intersections we can begin to make comparisons of efficiencies.

3.3 Comparison of Intersection Types

In this section we use our models of traffic lights and roundabout to investigate advantages and disadvantages of the respective intersection types. This is not simply a matter of running two simulations and plotting the results. There are many factors involved in how well a particular intersection type will work in a given situation. For instance, a particular traffic density could have an optimal choice of traffic light timing to maximize fuel efficiency, or possibly a different timing to maximize flow. Similarly,

for a roundabout there could be a circle size which is optimal for flow but not for fuel consumption. There is the added complexity of considering different drivers using the roundabouts. By changing the merger window size, F, the fuel efficiency and flux of the roundabout could change dramatically. These are all questions we will attempt to address in this section. The first thing we need is an accurate microscopic fuel consumption model.

3.3.1 Fuel Consumption Model

We apply a microscopic fuel consumption model which uses current vehicle speed and acceleration to compute a rate of fuel consumption. The fuel consumption model is referred to as "Model N" in [13] and is represented by the double sum in (3.6). Keeping the same notation as used in [13], MOE_e is the rate of fuel consumption in the units $\frac{Litres}{Hour}$, with "s" standing for speed in $\frac{meters}{second}$, and "a" for acceleration in $\frac{meters}{second^2}$. A detailed description of the parameters and the model derivation can be found in [13].

$$\log(MOE_e) = \sum_{i=0}^{3}\sum_{j=0}^{3}(k_{i,j} \cdot s^i \cdot a^j) \tag{3.6}$$

Model N does a very good job of approximating fuel consumption as can be seen in Figure 3.4. This plot shows Model N's predicted fuel consumption rate versus raw data. The raw data is represented by circles, and Model N's estimates are represented by stars. To attach a number to its accuracy a 10 minute test was conducted comparing Model N to raw fuel consumption data at every second. Of the 600 data points approximately 97% of the points had less than a 10% relative error with 76% having less than a 5% error. Model N will be used to attach a fuel consumption rate to our simulations of roundabouts and traffic lights which allows us to suggest which intersections are more efficient for both flux and fuel consumption.

3.3.2 Comparison setup

In this section we describe how we make comparisons between roundabouts and traffic lights. We will be using the intersection models described above with the assumption that cars will not make left turns. Both roundabouts and traffic light intersections have characteristics we can change causing an impact on overall effectiveness. The two we focus on here are roundabout size and traffic light timing. At certain densities

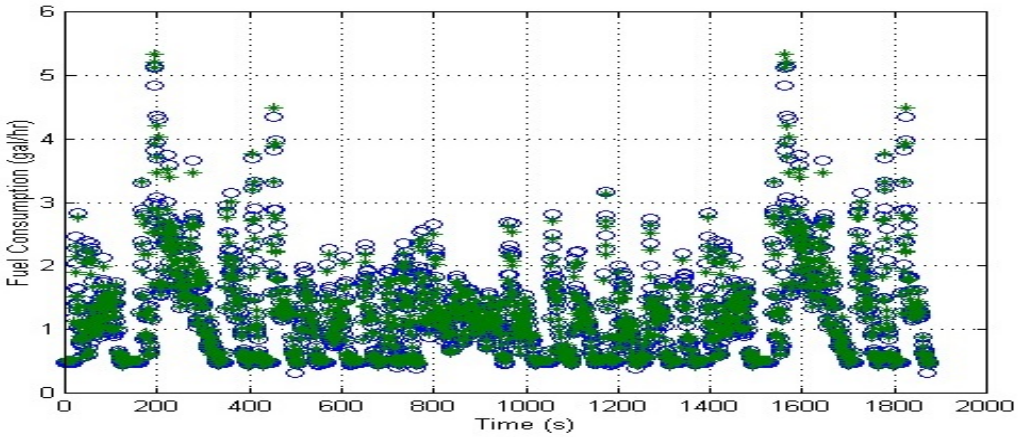

Figure 3.4: Examples of Model N compared to raw data, taken from [13].

it may be more effective to have a small roundabout versus a large roundabout, or short traffic light cycles versus long traffic light cycles. We conduct numerical tests to investigate how effectively these intersections handle low density or high density traffic in terms of flux and fuel efficiency.

The start of each simulation will be set up in the following way. All cars are placed on incoming roads and let go once the simulation starts with an initial speed set by a fundamental diagram. Measurements of fuel consumption begins on incoming roads 300 meters from the centre of the intersection with measurements ceasing at 300 meters past the intersection, or when the simulation ends. The results would be similar if we kept track of fuel consumption throughout the whole simulation, however, the difference between the intersections would become less pronounced, which is undesirable. Something which is not perfectly clear is where to start the lead car in each simulation. If we start the lead car at 300 meters from the centre of the intersection we get consistency from simulation to simulation. The downside is that it becomes difficult to set a particular traffic density at the intersection because the traffic would diffuse and speed up before it begins interaction with the intersection. Setting a particular density at the intersection can be achieved by starting the lead car close to the intersection, essentially retaining the initial density until interaction with the intersection begins. This has drawbacks of changing initial starting positions depending on the roundabout radius which affects travel distance of some vehicles in the simulation. Varying the density effectively changes two aspects of how cars interact with intersections. It changes both the spacing of the vehicles and how quickly they

are moving when arriving at the intersection. With this in mind we can simulate high density traffic interactions with intersections by capping the speed limit at a realistic speed for that density. By capping the speed limit and setting the initial density high we retain the high density and low speed as if traffic was congested throughout the whole road initially.

We will run each set of simulations 13 times and with each iteration we increase the duration of the light cycle and increase the radius of the roundabout. The smallest roundabout under consideration is 14 meters in radius, and with each iteration we increase its radius by 4 meters. A single lane roundabout with a 66 meter radius sounds unrealistically large and may indeed be unrealistic. There exist very large multilane roundabouts which are believed to produce better flux than single lane roundabouts. If this is true, then our results could be used as lower bounds on flux for these more sophisticated roundabouts. For traffic light intersections we start with a shortest cycle of 30 seconds. This equates to 15 seconds in the red phase, 10 seconds in the green phase and 5 seconds in yellow phase. With each iteration we increase the total cycle time by 8 seconds implying the longest cycle works out to be over 2 minutes in duration. For each length of cycle we keep the yellow phase at 5 seconds to ensure cars are able to stop in time. 5 seconds may sound a little long because most yellow lights last between 2 and 4 seconds. Usually for these intersections there is a brief period with all 4 lights red. Since we don't include this, we extend the yellow light to cover that time. We also made the assumption that as we increase the size of the roundabout we also increase the speed limit within the roundabout. For small roundabouts, $R < 20\,m$, we set the speed limit to $20\,km/h$. For medium sized roundabouts, $20\,m \leq R < 30\,m$, we set the speed limit to $30\,km/h$ and finally for large roundabouts, $R \geq 30\,m$, we set the speed limit to $40\,km/h$. Using this setup we begin testing how the intersections compare to each other as we vary their respective characteristics.

3.3.3 Comparison Results

The first set of numerical experiments was done by testing intersection effectiveness at low density. Low density here means incoming roads were set up to have an initial density of 0.05 with all traffic flowing at $50\,km/h$. As with all simulations, the lead car started 300 meters from the centre of the intersection. The results from this first set of simulations are shown in Figure 3.6. Results from the roundabout are plotted as

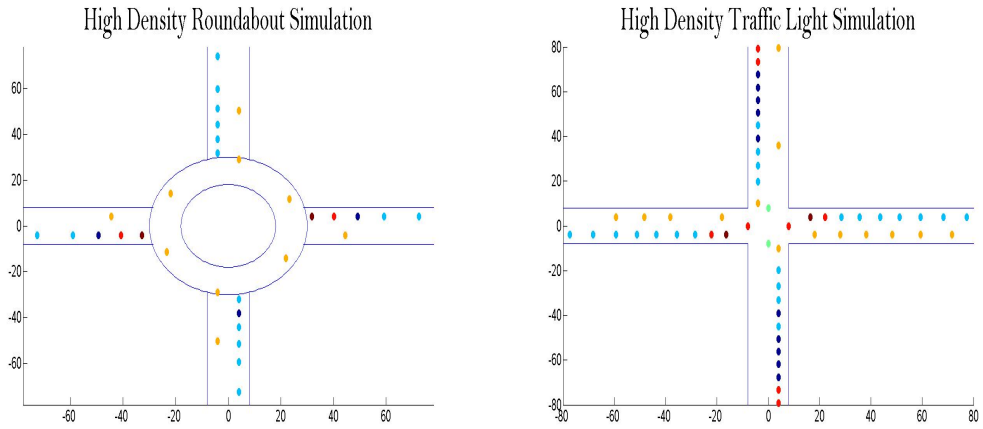

Figure 3.5: Intersections operating at high density

blue circles and traffic light results are plotted as green squares. The plot on the left shows the average fuel efficiency of a car at each iteration as we increase roundabout size and traffic cycle time. The plot on the right shows the flux from each iteration.

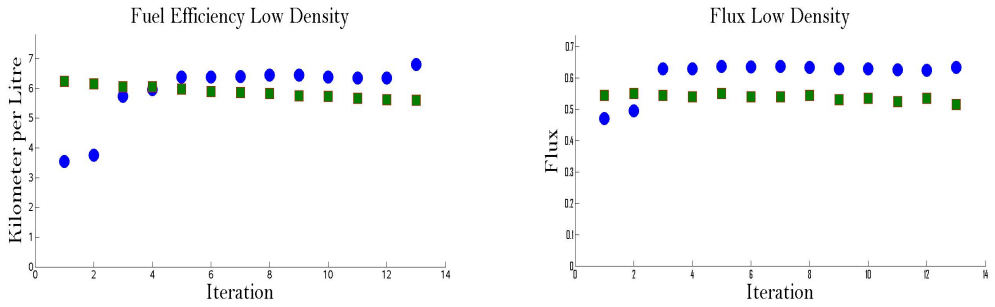

Figure 3.6: Low density KM/L per car and flux (right)

This first set of simulations exactly matches our intuition. When traffic is at low densities cars shouldn't have to sit and wait at an intersection. This is something which roundabouts accomplish and traffic lights don't. At low densities roundabouts allow cars to enter and exit without any extra decelerating or accelerating. With traffic lights, there is some luck involved with how long it may take to pass through. The car may arrive at a green light allowing immediate passage, or the light may be red requiring the driver to come to a full stop and then accelerate back up to speed. The latter is very inefficient, especially if there are no other cars using the intersection. We see these ideas reflected in the plotted results. We also see for small

roundabouts a slightly lower flux than for the medium and large roundabouts. This is to be expected with the roundabout's capacity being small because it increases the possibility of a car initially not having enough room to merge. To sum up we see traffic lights do significantly worse in both fuel efficiency and flux due to unnecessary waiting times at red lights.

The second set of numerical experiments is done by testing intersection effectiveness at a medium density. Medium density here implies incoming roads are set up to have an initial density of 0.2 with traffic maintaining a full speed of $50\,km/h$. The results from this second set of simulations are shown in Figure 3.7, with the same setup as discussed above.

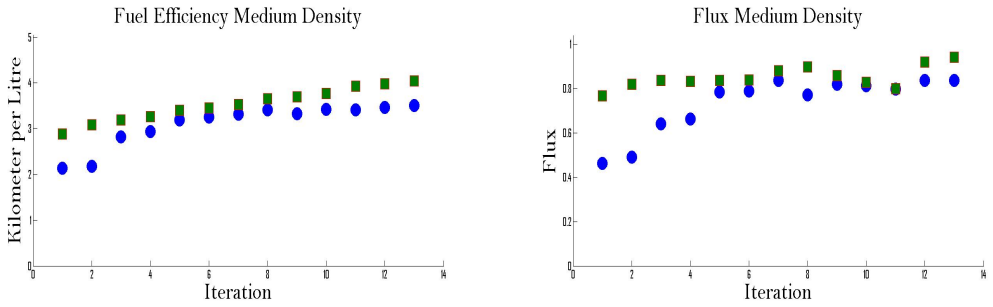

Figure 3.7: Medium density KM/L per car and flux (right)

For medium density traffic we see the traffic light intersection performs marginally better than the roundabout. As the roundabout size increases we see that the roundabout flux converge towards the values possessed by the traffic lights, however they still don't manage to do quite as well. The flux for the traffic light intersection contains a lot of variation which we believe is not due to the cycle length. Instead, we believe it is related to the actual timing of the lights relative to the initial conditions of traffic. The decrease in flux between iterations 8 and 11 is a consequence of this and should actually be increasing towards the top flux's shown in iterations 12 and 13. We see here that the top flux is achieved for traffic lights at the longest cycle length, but does this make sense? For arbitrary densities it is not clear whether or not to expect higher flux at longer light cycles. Each time a light switches from red to green it takes time for that lane of traffic to start flowing well. Now, suppose we have a 4-way traffic light intersection as used in our simulations. Also suppose, that the North-South lanes are experiencing optimal flux, with the other directions waiting at

a red light. Will this intersection increase its flux by switching the lights? No it will not, it simply cannot produce higher flux. Therefore, by switching the lights we lose flux due to the other lane not flowing optimally yet. It is important to note that this argument only works when the intersection is already operating at optimal flux. In the above simulation, we are at a density producing close to optimal flux, therefore it is not surprising to see a slight increase in flux as we increase cycle time.

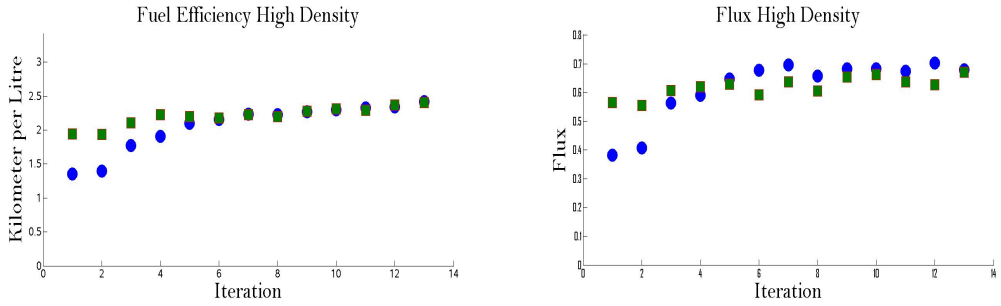

Figure 3.8: High density KM/L per car and flux (right)

The third set of numerical experiments is done by testing intersection effectiveness at high density. High density here implies incoming roads are set up to have an initial density of 0.42 with traffic grinding along at a sluggish $11\,km/h$. The results from this third set of simulations are shown in Figure 3.8, with the same setup as discussed above.

Unlike in low density traffic, it is unclear from the outset how changing roundabout radius and lengthening the light cycle will affect fuel efficiency and flux at high density. The results show that longer light cycles and larger roundabouts handle the high density traffic better in terms of both flux and fuel efficiency. Relative to each other, the roundabout has a slight edge in flux, with very similar fuel efficiencies.

Chapter 4

Macroscopic Modeling

4.1 Comparison to Macroscopic Traffic Models

Microscopic models are considered by some to possess higher accuracy than macroscopic models and are most useful for small scale modeling. The main issue with microscopic models is that they are computationally expensive once there are a large number of cars on the road. Macroscopic models were designed to deal with these large scale modeling problems, and they do an excellent job. These mathematical models use partial differential equations instead of ordinary differential equations and rely heavily on the theory of conservation laws. The most famous of the first order models is the Lighthill-Whitman and Richards Model (LWR), studied in [3,4], which uses the theory of scalar conservation laws. We begin our discussion of macroscopic models with the derivation of this model.

4.1.1 Derivation of the LWR model

Suppose we have a long stretch of road occupied by flowing traffic. Pick any two points on the road α and β with $\alpha < \beta$. We denote the local density at the point $x \in [\alpha, \beta]$ at time t by $\rho(x, t)$. Since the integral of density is mass we know the total number of cars in $[\alpha, \beta]$ is given by

$$\int_{\alpha}^{\beta} \rho(x,t)dx = \text{Number of cars in the section of road } [\alpha, \beta] \text{ at time t.} \tag{4.1}$$

Equation (4.1) is not the only way to calculate the total number of cars in $[\alpha, \beta]$ at time t. This quantity can also be computed as

$$\begin{aligned}\text{Total cars in } [\alpha,\beta] = {} & \text{total cars in } [\alpha,\beta] \text{ initially} + \text{total cars entering } [\alpha,\beta] \text{ up to time } t \\ & - \text{total cars leaving } [\alpha,\beta] \text{ up to time } t. \end{aligned} \tag{4.2}$$

Let $V(x,t)$ denote the speed of traffic at position x at time t. The total number of cars in $[\alpha, \beta]$ initially is given by $\int_\alpha^\beta \rho(x,0)dx$. The total number of cars which have entered $[\alpha, \beta]$ between $time = 0$ and $time = t$ is given by

$$\int_0^t \rho(\alpha,\tau)V(\alpha,\tau)d\tau \tag{4.3}$$

and the total number of cars which have left $[\alpha, \beta]$ between $time = 0$ and $time = t$

$$\int_0^t \rho(\beta,\tau)V(\beta,\tau)d\tau, \tag{4.4}$$

where $\rho(x,t)V(x,t)$ is referred to as the flux at position x at time t. Combining these quantities we now have the mathematical representation of (4.2) shown in (4.5).

$$\text{Total cars in } [\alpha,\beta] = \int_0^t \rho(\alpha,\tau)V(\alpha,\tau) - \rho(\beta,\tau)V(\beta,\tau)d\tau + \int_\alpha^\beta \rho(x,0)dx \tag{4.5}$$

Since equations (4.1) and (4.5) both describe the total number of cars in $[\alpha, \beta]$ at time t, we equate them to derive the equation

$$\int_\alpha^\beta \rho(x,t)dx = \int_0^t \rho(\alpha,\tau)V(\alpha,\tau) - \rho(\beta,\tau)V(\beta,\tau)d\tau + \int_\alpha^\beta \rho(x,0)dx. \tag{4.6}$$

Assuming that both the density and velocity functions are smooth we can rewrite the RHS of equation (4.6) as

$$\int_\alpha^\beta \rho(x,t)dx = \int_0^t \int_\alpha^\beta -\left(\rho(x,\tau)V(x,\tau)\right)_x dxd\tau + \int_\alpha^\beta \rho(x,0)dx. \tag{4.7}$$

Taking the derivative in time and using our smoothness assumption to take the derivative inside the LHS integral we get

$$\int_{\alpha}^{\beta} \rho_t(x,t)dx = \int_{\alpha}^{\beta} -\left(\rho(x,t)V(x,t)\right)_x dx. \tag{4.8}$$

$$\text{or, } \int_{\alpha}^{\beta} \rho_t(x,t) + \left(\rho(x,t)V(x,t)\right)_x dx = 0. \tag{4.9}$$

Since this quantity is zero for any choice of α and β with $\alpha < \beta$ the term inside the integral must be identically zero. This gives us the mass conservation law

$$\partial_t \rho(x,t) + \partial_x(\rho(x,t)V(x,t)) = 0. \tag{4.10}$$

For us to study this equation we need a single unknown quantity, the density ρ. If we want to apply this conservation law to traffic we would need the velocity function to be known, however, it simply is not. The LWR traffic model makes the assumption that the velocity of traffic is a function of the density. In other words, for any given density there will be a single velocity in which traffic will want to flow at. This is referred to as assuming a fundamental diagram and implies $V(x,t) = V(\rho)$. This turns (4.10) into

$$\partial_t \rho + \partial_x(\rho V(\rho)) = 0, \tag{4.11}$$

known as the LWR model. We discuss the fundamental diagrams in some detail in the next section. Another popular example of a macroscopic model comes from Aw and Rascle which builds on the work done by Lighthill and Whitman. They add a second equation to the LWR model creating a system of conservation laws. The second equation is known as the momentum equation and with its inclusion the model becomes,

$$\begin{aligned} \partial_t \rho + \partial_x(\rho V) &= 0, \\ \partial_t(V + p(\rho)) + V\partial_x(V + p(\rho)) &= 0. \end{aligned} \tag{4.12}$$

Notice how we no longer need to assume a fundamental diagram. This is because the second equation includes the velocity term, V, as a dependent quantity which can be solved for. This being said, many second order models include a relaxation term on the RHS of the momentum equation which includes a fundamental diagram. The term $p(\rho)$ seen in (4.12) is given and depends on the chosen model. A common choice

is $p(\rho) = c\rho^\gamma$, with c, $\gamma \in \mathbb{R}$.

4.2 The Fundamental Diagram

The fundamental diagram is a conjectured relationship between traffic velocity and traffic density used in macroscopic modeling. The first fundamental diagrams were suggested by Greenshields in 1934 with the assumption that velocity decreases linearly in density, with maximum velocity at minimum density and minimum velocity at maximum density. The corresponding parabolic relationship between flux and density is easily calculated and both are shown in Figure 4.1.

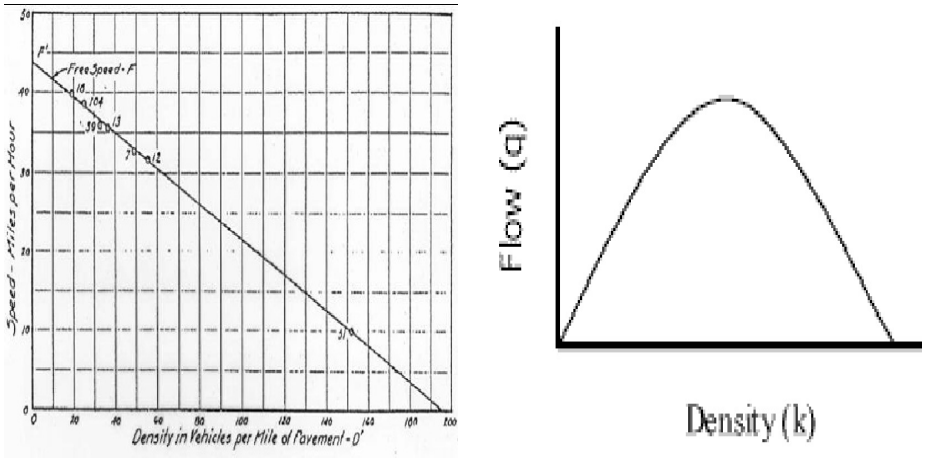

Figure 4.1: The first fundamental diagram by Greenshields in 1934.

Since Greenshields' model was introduced more sophisticated fundamental diagrams have been studied, each with their own strengths and weaknesses. Some examples include the multi-valued function used in the study of 3-phase flow seen in Figure 4.3, the steep hyperbolic tangent functions seen in Figure 4.2 and the commonly used slight variation on Greenshields' original model shown in Figure 4.2. Using a non-local traffic model, Illner and Herty in [9] studied the differences between multi-valued fundamental diagrams and the hyperbolic tangent function plotted in Figure 4.2. Overall, the resulting traffic predictions were similar, with the multi-valued function exaggerating certain aspects of traffic such the as formation of jams at bottlenecks. Qualitatively, however, the behaviour was very much the same. In a later section we compare different fundamental diagrams for the LWR model and we will see that resulting traffic dynamics rely heavily on the chosen diagram.

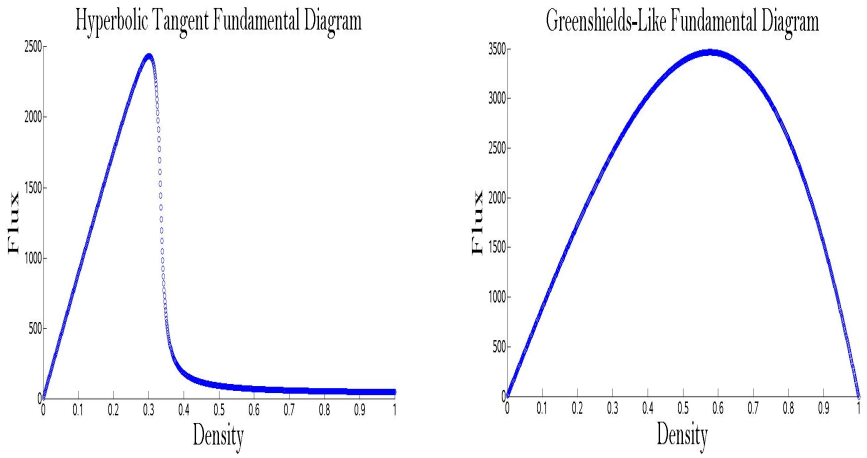

Figure 4.2: Two other fundamental diagrams.

All fundamental diagrams should have a linear portion starting from 0 density up to some critical value ρ_c. This indicates that in low densities cars do not interact with each other and hence, the flux should simply depend linearly on the density. How flux relates to density for values greater than this ρ_c is very dependent on the choice of diagram and even the particular situation. Many fundamental diagrams include a rather steep drop in flux at a particular density ρ_{jam} with $\rho_{jam} \geq \rho_c$. This steep drop in flux is consistent with observation and reflects the formation of traffic jams which are assumed to significantly reduce flux. This brings us to the focus of this section. How does the formation of jams impact flux? At what densities will jams begin to form? What would a fundamental diagram look like which reflects these results? In this section we will use our car interaction model to answer these questions.

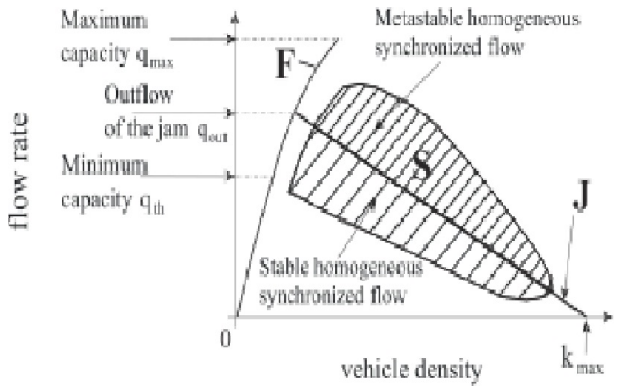

Figure 4.3: The fundamental diagram used in 3-Phase flow.

4.2.1 Formation of Jams and its Impact on Average Velocity

As shown in [12], traffic jams can form without a bottleneck, intersection or accident perturbing the flow. In particular, we are interested in jams which form from, what appears to be, smoothly flowing traffic. We think that the minimum density for which these jams will form is at ρ_{jam}, introduced above. Before we can justify this we need to show that the formation of these jams causes a decrease in average velocity.

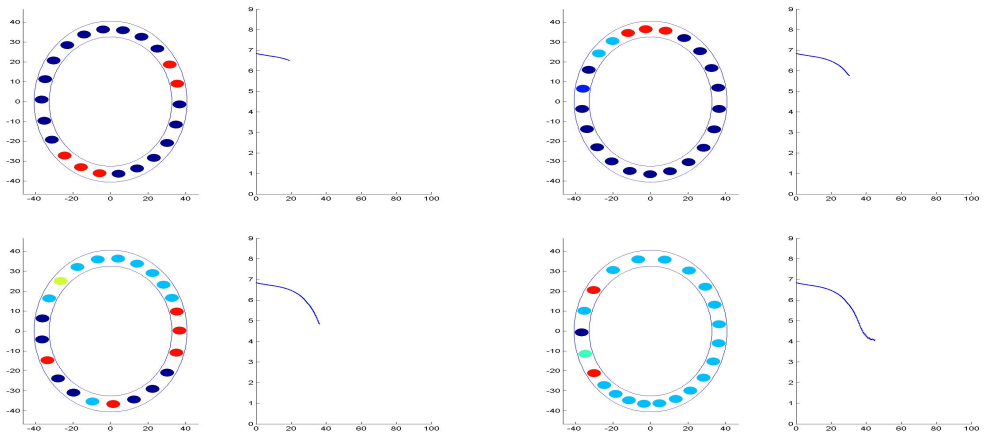

Figure 4.4: Jam formation reducing average speed.

Mimicking the experiment done in [12], we let 22 cars drive around a 230 meter track with the intent of driving $30km/h$ or roughly $9m/s$. The simulation starts with all vehicles traveling at roughly $7m/s$, with all cars evenly spaced out with a small amount of error. Figure 4.4 shows four different time steps of a simulation in chronological order from left to right, and top to bottom. Each of the four images depicts the cars in the circle on the left, and the average speed on the right. Initially, we see that the speed is slowly decreasing linearly in time. This is because some cars in the circle are braking and the density is too high for any car to accelerate beyond the initial $7m/s$. The first plot is at approximately 20 seconds into the simulation with the average speed slightly reduced from $7m/s$ to around $6.4m/s$, with no jams visible in the circle. The next plot is taken 10 seconds later with the first signs of a significant velocity drop but no signs of a jam. The third plot shows increased density at the top of the circle with continued drop in velocity and the final plot shows the high density on the bottom of the circle with average vehicle speed around $4m/s$.

The most significant aspect of this simulation is the reduction in average speed

and consequently the drop in flux. The reduction of average speed from nearly $7\,m/s$ to $4\,m/s$ means after the jam formed the flux was only 60% of what it was before the jam. With the formation of these jams causing a significant decrease in flux we expect the maximal flux over all possible densities will occur in a region where these jams are not forming. With these concepts in mind we look deeper into fundamental diagrams.

4.2.2 Applications to The Fundamental Diagram

In this section we use our car interaction model to compute a fundamental diagram from simulation results. We do this by running simulations similar to the experiment done in [12] for all possible densities and recording the average speed and flux. We hope to see a linear relationship between density and flux initially, and then a decrease as car interactions begin to impede the flow. Once jams start to form we expect a severe drop in flux as shown in the previous section. Each simulation contains 45 sub-simulations, each of which are run for 200 seconds. The first sub-simulation places one car on the 230 meter track and lets our microscopic model dictate its movement throughout the 200 seconds. The second sub-simulation, places two cars on the track and the third places three and so on. With the goal being to compute the average speed of traffic for a given density, we only keep track of vehicle speeds over the last 100 seconds. This removes the bias of the chosen initial speed, and gives a better approximation of what equilibrium speed traffic wants to flow at. This process is repeated up to the 45th sub-simulation, which corresponds to maximum density. Each set of 45 sub-simulations is run ten times with the results shown in Figure 4.5.

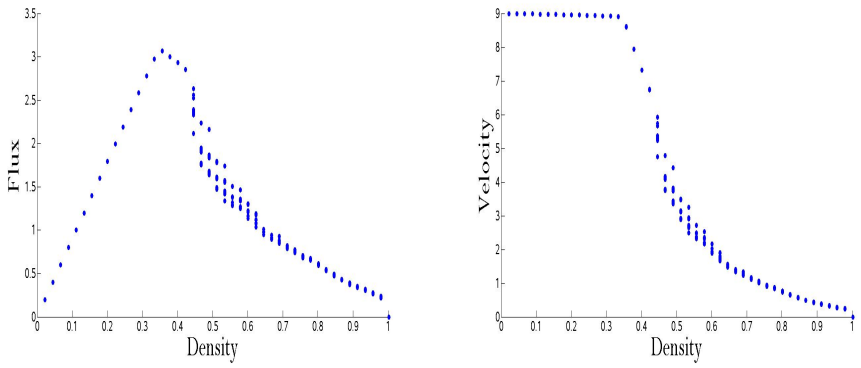

Figure 4.5: Results after 10 simulations for density vs. flux, and density vs. velocity.

There are two important things to notice about the results shown in Figure 4.5. The first thing is the expected linearity between flux and density for low densities. This is not overly profound, however, it matches our expectations of real traffic flow. The other interesting result is the variation in results between simulations. Notice for low densities, we have almost no variability. Again, this is because there are no car interactions in this regime, so small changes to the spacing between cars will not impact the resulting flux. This is not the case for densities between approximately 0.4 and 0.7. In fact, we see some simulations have almost half the flux of others with the difference in initial condition being extremely small. Traffic dynamics in this region of density are often referred to as "unstable", or essentially unpredictable, so the fact that our model shows this instability is rather promising. To extract a fundamental diagram from these results we simply average the fluxes at each density.

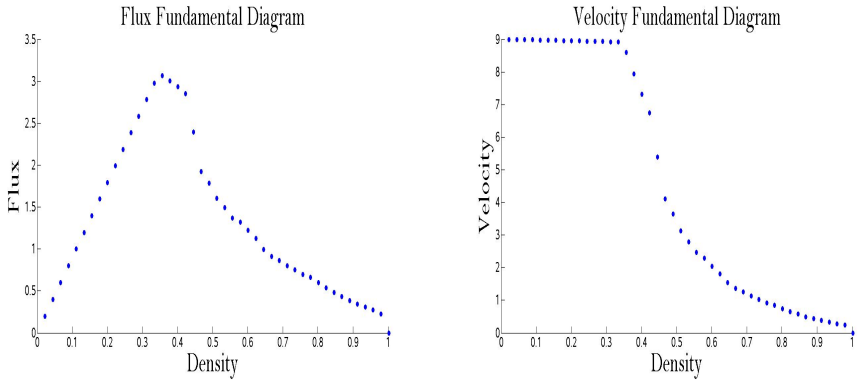

Figure 4.6: Computed fundamental diagrams.

The resulting fundamental diagram shown in Figure 4.6 captures all of the features we would look for in a realistic fundamental diagram. We see the linear density to flux relationship for low densities, the steep drop at $\rho_{jam} \approx 0.45$ and a smooth decrease to 0 flux as the density increases. One feature of this fundamental diagram we are pleased with is the short linearly decreasing section between approximate densities of 0.33 and 0.45. This is describing that between densities of 0.33 and 0.45 cars will have to reduce their speed due to interactions between one another, however, the reduction is not dramatic. Drivers frequently encounter these densities where they aren't going quite as fast as they would like, but traffic is still flowing smoothly. Recall that these results are for slower moving traffic, for example, traffic in a roundabout. This fundamental diagram does not simply translate to all types of roads. Notice in Figure 4.6 we have traffic maintaining the speed limit up to a density of approximately 0.33.

This means that if there is one car in every three car lengths traffic should be able to sustain maximum speed. This does not translate to all speed limits. If the speed limit is $80\,km/h \approx 22\,m/s$ this translates to drivers being comfortable less than half a second behind their leading car, which would be completely unsafe and unrealistic. So what does our model say for higher speed limits? First, we need to mention that our model is not calibrated for this type of traffic, although, we can extract some general features from it. In Figure 4.7 we show the velocity fundamental diagram predicted for highway type traffic. The speed limit is taken as $80\,km/h$ and all other model parameters are left as in previous simulations.

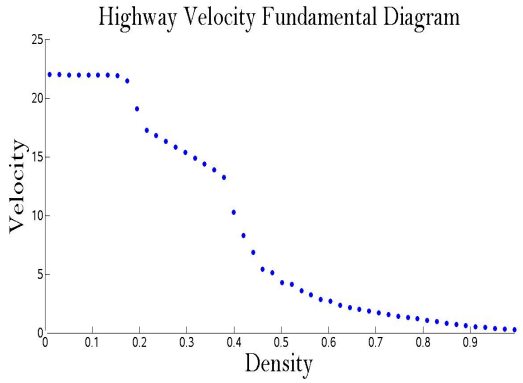

Figure 4.7: Computed fundamental diagram for highway speeds.

Our goal here is not to analyze every aspect of this result because we have not validated our model at these speeds. The question that brought us here is whether or not the fundamental diagrams should be the same for all speed limits. The obvious answer is no, the check on comfort distance was enough to answer that question. We see that this is addressed by our model. Notice in Figure 4.7 that the maximum speed is only sustained up to density 0.17, a significant change from the 0.33 which our roundabout fundamental diagram predicts. Our model shows this earlier drop in velocity through the aggressive driving condition. Recall that a driver will ignore the speed of their leading vehicle if $H + \widetilde{T} \cdot u_i(t-\tau) < c_4(x_{i-1}(t-\tau) - x_i(t-\tau))$, where H is the minimum safety distance and $\widetilde{T} \cdot u_i(t-\tau)$ is the distance traveled in $\widetilde{T}$ seconds. Suppose we have a car traveling at the speed limit, $U_{max} = 9\,m/s$, then at what distance does their leading car need to be for the aggressive driving term to take over? Using our calibrated parameters of $H = 7.12$, $\widetilde{T} = 2$ and $c_4 = 1.7$, we get $7.12 + 2 \cdot 9 < 1.7 \cdot (x_{i-1}(t-\tau) - x_i(t-\tau))$. Dividing by the 1.7 we see that if $(x_{i-1}(t-\tau) - x_i(t-\tau)) > 14.77$ the ith car will accelerate towards the speed limit.

Thinking in terms of local density, $\rho_{local} = \frac{L}{x_{i-1}(t-\tau)-x_i(t-\tau)}$, we can rewrite this aggressive driving condition as,

Accelerate towards the speed limit if

$$\rho_{local} < c_4 \cdot \frac{L}{H + \widetilde{T} \cdot u_i(t-\tau)}.$$

Plugging in our numbers from above we see that the car will accelerate towards the speed limit if $\rho_{local} < \frac{5.12}{14.77} = 0.34$. Referring to Figure 4.6 we see that this is exactly the density at which the average speed begins to decrease from U_{max}. Essentially, if all drivers continue to perceive that they have enough space to accelerate to the speed limit, then eventually all cars will be going the speed limit. This implies that we have control over where the decrease in speed begins directly through the choice of c_4. If we repeat this calculation for the highway speeds of $U_{max} = 80\,km/h$ we see that cars will accelerate towards the speed limit if $\rho_{local} < \frac{5.12}{30.07} = 0.17$, which again matches the decrease in speed shown in Figure 4.7. A local density of 0.17 corresponds to 30.07 meters between cars. This may seem a little close because a car traveling at $22\,m/s$ will cover that distance in 1.36 seconds. This is not the usual 2 second rule that most drivers go by, however, as mentioned in our calibration section we needed to make these drivers more aggressive than expected to get the desired results. In fact, if we repeat this distance calculation for our calibrated speed limit $U_{max} = 9\,m/s$, we see a local density of 0.34 corresponds to a distance of 14.77 meters. A car traveling at $9\,m/s$ covers 14.77 meters in 1.64 seconds which also violates the 2 second rule. We are unable to comment on the accuracy of this specific fundamental diagram or if all of its features make sense. We do know that the earlier drop from maximum velocity matches our expectations and the smooth decrease down to zero velocity looks reasonable.

Before leaving this topic, it seems natural to ask if there exists a relationship between fuel consumption and density similar to the one between flux and density. The first thing we need to do is clarify what we mean by fuel consumption. There are two important quantities to consider when discussing fuel consumption namely, the rate at which a car is consuming fuel, given in the units $\frac{Litres}{Hour}$, and the second being fuel efficiency, given in the units $\frac{Kilometers}{Litre}$. In this section we mostly deal with the rate of fuel consumption.

Intuitively we expect total fuel consumption per unit time to increase with the

number of cars on the road. Is this necessarily correct? How does density affect the average fuel consumption per car? Does the goal of minimizing fuel consumption on a roadway counteract the goal of maximizing flux? To try and answer these question we rerun the same 10 simulations as we did in our fundamental diagram investigation, except this time we keep track of fuel consumptions.

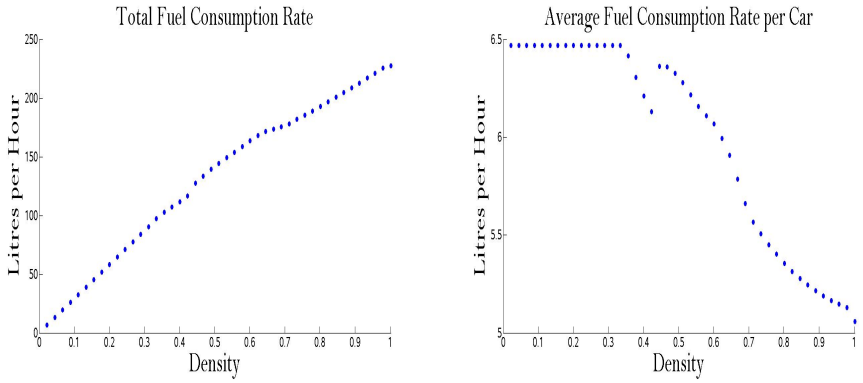

Figure 4.8: Total fuel consumption rate, and fuel consumption rate per car

The first batch of results is shown in Figure 4.8. The plot on the left is the total fuel consumption rate averaged over the ten simulations and on the right is the average fuel consumption rate per car averaged over the ten simulation. The most noticeable feature is the large jump in the fuel consumption per car at ρ_{jam}. This is no surprise. The fuel cost of accelerating is significantly more than the cost of maintaining a constant speed. With the formation of jams starting we get significantly more switching between acceleration and deceleration than in lighter traffic. If a bad jam forms with fewer cars in the circle this allows the cars to accelerate up to full speed then slow back down soon after. This is highly inefficient! Notice that cars in lows density traffic are consuming roughly $\frac{6.5L}{Hr}$, and that the cars in high densities are consuming roughly $\frac{5L}{Hr}$. Are we saying traffic at high density isn't bad for fuel consumption? Absolutely not, this is where fuel efficiency becomes important. Yes, when a car is in very heavy traffic it is essentially idling, which means it is consuming fuel at a very low rate. But, as we know from our fundamental diagrams, this traffic is also moving very slowly. Therefore, the $\frac{KM}{L}$ will be very low causing a larger amount of fuel to be consumed overall. With this in mind we can incorporate traffic speed into the analysis of fuel consumption.

Figure 4.9 is a plot of $\frac{\text{Kilometers}}{\text{Litre}\cdot\text{ Cars}}$, the number of kilometers on average a car will

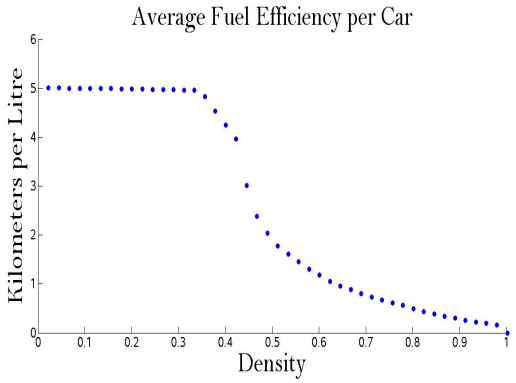

Figure 4.9: Fuel efficiency per car in KM/L

travel per litre of fuel consumed. This quantity is easily derived from our fuel consumption rate. Suppose we have a car consuming fuel at some rate. This rate of fuel consumption can be expressed in two ways, either as $\frac{L}{Hr}$ or $\frac{Hr}{L}$. Although these numbers will be different, they are telling us the same thing. One is saying how many litres a car will burn in an hour, given as $\frac{L}{Hr}$, and the other is saying how many hours a car can drive per litre of gas, given as $\frac{Hr}{L}$. We choose to work with $\frac{Hr}{L}$ since it ends up presenting the resulting information in a more convenient way. Taking this quantity for fuel consumption rate, we multiply it by the vehicle speed given in $\frac{KM}{H}$, giving us the resulting units $\frac{Hr \cdot KM}{L \cdot Hr} = \frac{KM}{L}$. The largest values in Figure 4.9 correspond to the farthest distance traveled for the least fuel, or very efficient driving, and low values correspond to the least distance traveled per amount of fuel, or inefficient driving. Similar to the velocity fundamental diagram we see a constant up to ρ_c. This is a result of cars not interacting, therefore the fuel consumption raises at the same rate as the sum of vehicle speeds. At ρ_{jam} we see a very steep drop because the velocity is quickly decreasing as the fuel consumption per car stays fairly high, as seen in Figure 4.8. This plot also confirms that slow moving traffic, although consuming less fuel per unit time, is overall significantly less efficient in the long run. An interesting result here is how similar the $\frac{\text{Kilometers}}{\text{Litres} \cdot \text{Cars}}$ looks to the velocity fundamental diagram in Figure 4.6. This similarity can be interpreted as the optimization of flux on a roadway will automatically give you the best fuel efficiency in the process. The resulting fuel consumption fundamental diagram (FCFD) would be the average fuel consumption rate per car, shown in Figure 4.9. This could give macroscopic modelers a quick way to estimate fuel consumption based on density and attach a specific cost to a given traffic scenario. If a macroscopic traffic model is used to show how improvements to

a roadway can improve flux the FCFD could be used as a cost analysis tool. Before the FCFD can be applied in these situations it needs to be tested for accuracy.

4.3 Density Evolution

In this section we focus on using the car interaction model and simulation results to derive quantities more comparable to macroscopic traffic modeling. As mentioned before, macroscopic traffic models focus on the evolution of density and not the motion of individual cars. Ideally, we would like to be able to compare our microscopic results to macroscopic results; however, the current format of our results don't allow us to make such comparisons. In this next section we develop numerical techniques to derive approximate vehicle distributions from density data.

4.3.1 Numerical Approach

The goal here is to develop a numerical technique for comparing microscopic to macroscopic models. We do this by taking the initial traffic density distribution, required for the macroscopic model to begin predicting traffic conditions, and extracting vehicle positions corresponding to the density distribution. With the estimated vehicle positions we can run our microscopic traffic model for the same length of time as the macroscopic prediction. At this point a comparison can be made it two ways: One way would be to again extract the vehicle position from the macroscopic density distribution to compare positions of cars microscopically, or we can approximate a density from the microscopic model to compare to the macroscopic prediction. These concepts are straightforward, but we need to ensure that we have a clear understanding of how to accurately extract vehicle position from the density.

The macroscopic density, $\rho(x,t)$, can have several interpretations, some of which make our goal of transitioning to microscopic fairly ill-conditioned. There is however, one popular interpretation which is convenient for our purposes. Here, the macroscopic density at a point is simply taken as the inverse of the average distance to the next car down the road. Microscopically, we can think of this as the average number of cars in some unit length, in other words, if car i looks ahead one car length, how many cars should they expect to see? Does this make sense? Suppose traffic is bumper to bumper, maximum density, then macroscopically this would imply $\rho = 1$. If we switch to thinking microscopically, car i should expect to see exactly one car

if they look one car length ahead. For this particular situation the macroscopic to microscopic interpretation is consistent with what we expect. Given that we understand how to compare these two idea of densities, we need a method of transforming a density distribution into car placement.

Suppose over a given section of road $[a, b]$ we have a density distribution $\rho(x, t_0)$ as seen in Figure 4.10. Since we want to use a microscopic traffic model on this data we need positions of individual cars on the road. Using that the integral of density is mass, we search for the largest point $x_1 \in [a, b]$ such that $\int_{x_1}^{b} \rho(x, t_0)dx = L$. This is a simple root finding problem for the function $f(x, t_0) = \int_{x}^{b} \rho(x, t_0)dx - L$.

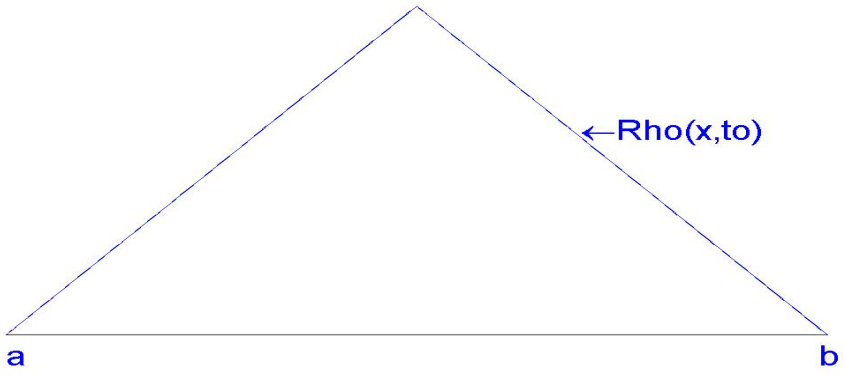

Figure 4.10: Sample density distribtion

In Figure 4.10 we have a road length of 200 meters with $a = 0$ and $b = 200$, with the initial density distribution defined as the simple piecewise function,

$$\rho(x, t_0) = \begin{cases} .008(x - 100) + 0.8, & \text{if } x \leq 100 \\ .008(100 - x) + 0.8, & \text{if } x > 100. \end{cases} \tag{4.13}$$

In this case, finding the x_1 such that $f(x_1, t_0) = 0$ is simple and can be done by hand. Assuming that $L = 5$ we solve the following problem for x_1

$$\int_{x}^{200} \rho(x, t_0)dx - L = 0.$$

Where $\rho(x, t_0)$ is defined as in (4.13). With some basic integration we get

$$-0.004(x-100)^2 + 0.8x\Big|_{x_1}^{200} - L = 0$$
$$-0.004(100)^2 + 80 - (-0.004(x_1-100)^2 + 0.8x_1) - L = 0$$

After some simplifying, we derive the quadratic

$$0.004x_1^2 - 1.6x_1 + 155 = 0$$

which has roots at $x_1 = 164.644, 235.355$. We want the first root, $x_1 = 164.644$, because the other root is not in our domain. This first region is plotted in Figure 4.11.

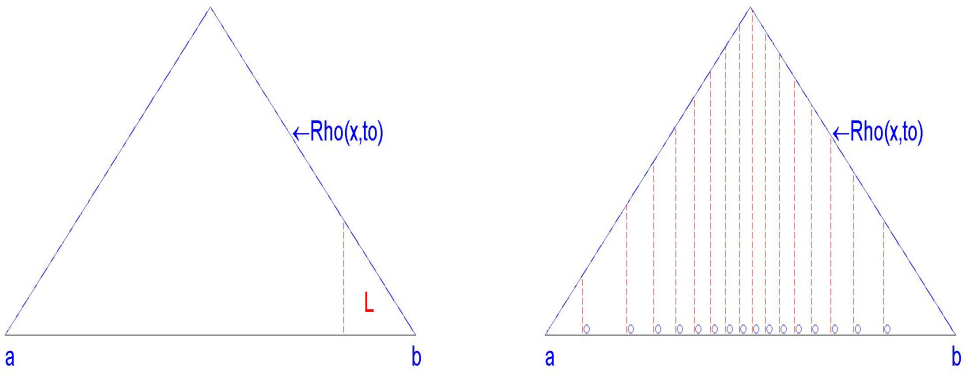

Figure 4.11: Placing the cars

By finding x_1 we have a section of the road, $[164.44, 200] \in [0, 200]$, which contains our leading vehicle. This brings us to our first dilemma. By the definition of density which we are using, we expect there a be car somewhere in this interval; however, to use our microscopic model we need the exact position of this car. To deal with this we simply choose the position of the first car so that its back bumper is on the point x_1. This is not the only choice; in fact, we could put this car anywhere in $[164.44, 200]$ and we would still be using our definition of density correctly.

Once we have found the placement of car i at, $x_i \in [a, b]$, we place the next car, indexed by i+1, at the relevant root of the equation $f(x_{i+1}, t_0) = \int_{x_{i+1}}^{x_i} \rho(x, t_0)dx - L$. This process is repeated N times where $\int_{x_N}^{x_{N-1}} \rho(x, t_0)dx = L$ and $\int_a^{x_N} \rho(x, t_0)dx < L$. The final placement of all the N cars is plotted in Figure 4.11.

Another dilemma this method can run into is a lack of complete definition of the density $\rho(x, t)$. Often when modeling with pde's the density is only defined on a subset of the road known as a grid. The grid is usually defined in terms of equally spaced points along the domain with the distance between points determined by the time step, the required accuracy and how much computation power is available. In some situations the domain can be several kilometers long, meaning the grid points could be several meters apart. If the grid points are this far apart it may be impossible to get even a single digit of accuracy with the root finding problem. To deal with this problem an interpolation technique can be used to extract a much finer grid than used by the macroscopic model. This would allow for higher accuracy on car placement without impacting the macroscopic simulation.

4.3.2 Microscopic to Macroscopic Comparison

Now that we have developed a method for extracting car positions from a density profile, we are able to make direct comparisons of macroscopic and microscopic traffic models. For simplicity, we compare our microscopic model (2.2) to the basic LWR model (4.11) derived above. There are three main things we wish to accomplish with these comparisons. First, we want to apply the density to car placement method to ensure its validity. Second, we want to compare how the two models predict traffic conditions, and finally we want to investigate which fundamental diagram causes the macroscopic predictions to best match the microscopic predictions. This raises an interesting question; why compare the two models if we don't know which model is correct? Yes, we do not have overwhelming evidence that (2.2) accurately predicts highway traffic flow; however, we do know that it is quite reliable when it comes to reproducing the circle experiment studied in [12]. With this in mind, we will perform all of the comparisons on a circular track at low speeds, meaning we must induce periodic boundary conditions on the macroscopic model.

We will run the comparisons on a circular track with circumference $\mathcal{D}$ and speed limit U_{max}. We take the initial density distribution $\rho(x, 0)$ with $x \in [0, \mathcal{D}]$ and set $\rho(0, t) = \rho(\mathcal{D}, t)$ since the domain is a circle. We partition the spatial domain, $[0, \mathcal{D}]$,

into $\mathcal{M}$ equally spaced points distance Δx apart. This implies $0 + \mathcal{M} \cdot \Delta x = \mathcal{D}$. Working towards an accurate numerical approximation of the LWR model we recall the conservative form of the LWR model,

$$\partial_t \rho + \partial_x(\rho V(\rho)) = 0.$$

For simplicity we let $q(x,t) = \rho(x,t)V(\rho(x,t))$, where $q(x,t)$ is known as the flux function. We estimate $\frac{\partial \rho(x,t)}{\partial t}$ using the forward Euler method in time, giving

$$\frac{\partial \rho(x,t)}{\partial t} \approx \frac{\rho(x, t+\Delta t) - \rho(x,t)}{\Delta t}.$$

We need to be much more careful with the spatial derivative, because depending on the choice of scheme, the results can vary wildly. The most popular choice among first order schemes is the upwind scheme. The advantage of this scheme is its simplicity to implement and its stability, for linear problems, if the Courant-Friedrichs-Lewy condition, or CFL condition, is satisfied. Suppose we have a grid point, x, and want to compute the value at the next time step, $u(x, t + \Delta t)$. In the true solution, the evolution of this point, between t and $t + \Delta t$, will be affected by some domain of neighboring points. This set of points which influences the motion of the particle is known as the domain of dependence at x between times t and $t + \Delta t$. The CFL condition ensures that the domain of dependence for the true solution is a subset of the numerical domain of dependence. For the upwind scheme, the CFL condition ensures that information cannot travel farther than a grid point at each step. If This idea is nicely illustrated through the one-dimensional linear wave equation shown in (4.14).

$$\frac{\partial u}{\partial t} + a \cdot \frac{\partial u}{\partial x} = 0. \tag{4.14}$$

Equation (4.14) describes the wave propagation in direction x at velocity a. The distance a wave will travel in Δt seconds traveling at velocity a is $a \cdot \Delta t$. To ensure it does not travel farther than a grid point, we set $a \cdot \Delta t \leq \Delta x$. Therefore, the upwind scheme for the one-dimensional linear wave equation satisfies the CFL condition if

$$\left| a \cdot \frac{\Delta t}{\Delta x} \right| \leq 1. \tag{4.15}$$

We take a similar approach to get the CFL condition for the scalar conservation law.

Using the chain rule we rewrite (4.11) as

$$\frac{\partial \rho}{\partial t} + \frac{\partial q}{\partial \rho}\frac{\partial \rho}{\partial x} = 0. \tag{4.16}$$

Setting $a(\rho) = \frac{\partial q}{\partial \rho}$, we have our scalar conservation law looking very similar to the linear one-dimensional wave equation (4.14). The only difference is that the wave speed, a, is a function of the density. Therefore, the CFL condition is satisfied if $\left|\sup_{\rho} a(\rho) \cdot \frac{\Delta t}{\Delta x}\right| \leq 1$, which is a necessary condition for stability. Assuming we have chosen our CFL condition appropriately, we now apply the upwind scheme to (4.16).

We first move the spatial derivative over to the RHS and use forward Euler on the time derivate giving

$$\rho_i^{n+1} = \rho_i^n - \Delta t \cdot a(\rho_i^n)\frac{\partial \rho_i}{\partial x},$$

where ρ_i^{n+1} denotes the density at position i at time $n+1$. What makes upwinding more effective than a basic Euler method is it uses the wave direction to help choose the proper direction of finite difference. The scheme is as follows
If $a(\rho_i^n) > 0$, then

$$\rho_i^{n+1} = \rho_i^n - \Delta t \cdot a(\rho_i^n)\frac{\rho_i^n - \rho_{i-1}^n}{\Delta x},$$

otherwise

$$\rho_i^{n+1} = \rho_i^n - \Delta t \cdot a(\rho_i^n)\frac{\rho_{i+1}^n - \rho_i^n}{\Delta x}.$$

In the case of the scalar conservation law $a(\rho) = \frac{\partial q}{\partial \rho}$, therefore, this also needs to be approximated using finite differences. Using a finite difference scheme for $a(\rho)$ we write our upwind scheme in its final form

$$\rho_i^{n+1} = \rho_i^n - \frac{\Delta t}{\Delta x}\cdot\left(\max\left(\frac{q_{i+1}^n - q_i^n}{\rho_{i+1}^n - \rho_i^n}, 0\right)\cdot(\rho_i^n - \rho_{i-1}^n) + \min\left(\frac{q_{i+1}^n - q_i^n}{\rho_{i+1}^n - \rho_i^n}, 0\right)\cdot(\rho_{i+1}^n - \rho_i^n)\right).$$

Although the upwinding scheme is nice and stable it is sometimes too diffusive. To avoid the issue of too much diffusion some second order models are used such as the Lax-Wendroff scheme,

$$\rho_i^{n+1} = \rho_i^n - \frac{\Delta t}{\Delta x}(q_{i+1}^n - q_{i-1}^n) + \frac{\Delta t^2}{\Delta x^2}\left(A_{i+\frac{1}{2}}(q_{i+1}^n - q_i^n) - A_{i-\frac{1}{2}}(q_i^n - q_{i-1}^n)\right), \tag{4.17}$$

where $A_{i+\frac{1}{2}} = \frac{q_{i+1}^n - q_i^n}{\rho_{i+1}^n - \rho_i^n}$ and $A_{i-\frac{1}{2}} = \frac{q_i^n - q_{i-1}^n}{\rho_i^n - \rho_{i-1}^n}$.

The issue with many second order schemes, including this one, is that they are

dispersive. Dispersion in these schemes shows up as oscillations at shocks or other discontinuities in the data. Since discontinuities in our data are likely to occur, we need to control the dispersion in these higher order methods. This is done through a type of method called a high-resolution method. These methods are designed to combine the strengths of the upwind scheme and second order schemes. This achieves accuracy at shocks or discontinuities, and second order accuracy where the data is smooth removing any incorrect diffusion or dispersion. The most common type of the high-resolution methods are known as flux-limiter methods. The numerical scheme is generally expressed in terms of the flux at cell edges, as shown in (4.18). The ith cell has density at the left edge $\rho_{i-\frac{1}{2}}$ and density at right edge $\rho_{i+\frac{1}{2}}$.

$$\rho_i^{n+1} = \rho_i^n - \frac{\Delta t}{\Delta x}\left(Q(\rho_{i+\frac{1}{2}}^n) - Q(\rho_{i-\frac{1}{2}}^n)\right). \tag{4.18}$$

We let $q_{i+\frac{1}{2}}^{n,high}$ denote the flux at the right cell edge as calculated by the higher resolution scheme. In our case $q_{i+\frac{1}{2}}^{n,high}$ would denote the flux on the ith cell's right edge as calculated by $high\,resolution$ Lax-Wendroff scheme (4.17). Similarly, $q_{i+\frac{1}{2}}^{n,low}$ denotes the flux on the ith cell's right edge as calculated by the $low\,resolution$ upwind scheme. We define the flux at cell edges as

$$\begin{aligned} Q(\rho_{i+\frac{1}{2}}^n) &= q_{i+\frac{1}{2}}^{n,low} - \phi(\theta_i)\left(q_{i+\frac{1}{2}}^{n,low} - q_{i+\frac{1}{2}}^{n,high}\right) \\ Q(\rho_{i-\frac{1}{2}}^n) &= q_{i-\frac{1}{2}}^{n,low} - \phi(\theta_{i-1})\left(q_{i-\frac{1}{2}}^{n,low} - q_{i-\frac{1}{2}}^{n,high}\right), \end{aligned}$$

where ϕ is called the flux limiter. $\theta_i = \frac{\rho_{i'+1} - \rho i'}{\rho i+1 - \rho i}$ gives the ratio of gradients for successive cells in the upwind direction, with $i' = i - sgn(A_{i+\frac{1}{2}})$. θ's job is to measure how steep the solution curve is, and ϕ's job is to decide which of the high or low resolution schemes is best suited for the situation. Immediately, we observe that when $\phi(\theta_i) = 0$ the flux at right cell edge is given exactly by the low resolution scheme, $Q(\rho_{i+\frac{1}{2}}^n) = q_{i+\frac{1}{2}}^{n,low}$. If $\phi(\theta_i) = 1$, the $q_{i+\frac{1}{2}}^{n,low}$'s cancel out and the flux on the right cell edge becomes exactly the high resolution flux $Q(\rho_{i+\frac{1}{2}}^n) = q_{i+\frac{1}{2}}^{n,high}$.

There are many choices for the limiter function ϕ and finding the right one for a specific problem can be a bit of a trial and error process. A basic flux limiter is called the van Albada 2 limiter and we quickly analyze it to get a feel for how these limiter functions work.

The van Albada 2 limiter is defined as

$$\phi_{VanAlb2}(\theta_i) = \frac{2\theta_i}{\theta_i^2 + 1}. \tag{4.19}$$

Recall that θ_i is the estimation of the smoothness between cell i and its upwind adjacent cell. $\theta_i \approx 1$ implies the adjacent cells have a similar change in density over their respective cells. This is how our scheme interprets smoothness. If $\theta_i << 1$ or $\theta_i >> 1$ it means the change in density over one the cells is dramatically different than the other. This is sometimes referred to as a kink in the data, and the scheme would interpret this is being not smooth. If we take our smooth data, $\theta_i \approx 1$, and plug it into $\phi_{VanAlb2}$ we get a number which is still close to 1. This is good because this puts emphasis on $q_{i+\frac{1}{2}}^{n,high}$, the high resolution flux function. If instead, θ_i interprets kinked data, for example $\theta_i >> 1$, we get $\phi_{VanAlb2}$ close to 0 putting emphasis on $q_{i+\frac{1}{2}}^{n,low}$, the low resolution scheme as seen above. Similarly for $0 < \theta_i << 1$. The last option is $\theta_i < 0$ which could occur at a local extrema in the data. In this situation we take $\phi_{VanAlb2} = 0$ to avoid the high resolution method causing an increase in total variation. An advantage of flux-limiter methods is they are total variation diminishing, (TVD), which implies the total variation is non-increasing as time evolves. This is a desirable property for numerical approximations of scalar conservation laws because the true solution is also TVD.

Now that we have an understanding of how flux-limiter methods work we use the upwind scheme as the low resolution scheme and Lax-Wendroff as the high resolution scheme. We begin putting together our numerical scheme.

To start off, we define $q_{i+\frac{1}{2}}^{n,low}$ and $q_{i+\frac{1}{2}}^{n,high}$, the low and high resolution flux at the right cell edge. $q_{i+\frac{1}{2}}^{n,low}$ represents the flux from the upwind scheme on the right cell edge. An equivalent version of the upwind scheme is given by

$$\rho_i^{n+1} = \rho_i^n - \frac{\Delta t}{\Delta x} \begin{cases} q_i^n - q_{i-1}^n, & \text{if } a(\rho_i^n) > 0 \\ q_{i+1}^n - q_i^n, & \text{if } a(\rho_i^n) < 0. \end{cases}$$

Therefore, the flux on right cell edge depends on the wave direction giving

$$q_{i+\frac{1}{2}}^{n,low} = \begin{cases} q_i^n, & \text{if } a(\rho_i^n) > 0 \\ q_{i+1}^n, & \text{if } a(\rho_i^n) < 0. \end{cases} \tag{4.20}$$

Similarly for the flux on the left cell edge

$$q_{i-\frac{1}{2}}^{n,\,low} == \begin{cases} q_{i-1}^{n}, & \text{if } a(\rho_i^n) > 0 \\ q_i^n, & \text{if } a(\rho_i^n) < 0. \end{cases} \tag{4.21}$$

We derive the quantities $q_{i+\frac{1}{2}}^{n,\,high}$ and $q_{i-\frac{1}{2}}^{n,\,high}$ by working with equation (4.18) and exploiting the result that when $\phi = 1$ the scheme uses purely the high resolution scheme. We can rewrite equation (4.18) as

$$\rho_i^{n+1} = \rho_i^n - \frac{\Delta t}{\Delta x}\left(q_{i+\frac{1}{2}}^{n,\,low} - \phi(\theta_i)\left(q_{i+\frac{1}{2}}^{n,\,low} - q_{i+\frac{1}{2}}^{n,\,high}\right) - \left(q_{i-\frac{1}{2}}^{n,\,low} - \phi(\theta_{i-1})\left(q_{i-\frac{1}{2}}^{n,\,low} - q_{i-\frac{1}{2}}^{n,\,high}\right)\right)\right). \tag{4.22}$$

Taking $\phi = 1$,

$$\rho_i^{n+1} = \rho_i^n - \frac{\Delta t}{\Delta x}\left(q_{i+\frac{1}{2}}^{n,\,high} - q_{i-\frac{1}{2}}^{n,\,high}\right).$$

Equating this with the Lax-Wendroff scheme we get

$$q_{i+\frac{1}{2}}^{n,\,high} - q_{i-\frac{1}{2}}^{n,\,high} = \frac{q_{i+1} - q_{i-1}}{2} - \frac{\Delta t}{2\Delta x}\left(a(\rho_{i+\frac{1}{2}}^n)(q_{i+1}^n - q_i^n) - a(\rho_{i-\frac{1}{2}}^n)(q_i^n - q_{i-1}^n)\right).$$

Adding and subtracting $\frac{q_i}{2}$ to the RHS

$$q_{i+\frac{1}{2}}^{n,\,high} - q_{i-\frac{1}{2}}^{n,\,high} = \frac{q_{i+1} - q_i}{2} + \frac{q_i - q_{i-1}}{2} - \frac{\Delta t}{2\Delta x}\left(a(\rho_{i+\frac{1}{2}}^n)(q_{i+1}^n - q_i^n) - a(\rho_{i-\frac{1}{2}}^n)(q_i^n - q_{i-1}^n)\right).$$

Collecting the $(q_{i+1}^n - q_i^n)$ and $(q_i^n - q_{i-1}^n)$ terms together,

$$q_{i+\frac{1}{2}}^{n,\,high} - q_{i-\frac{1}{2}}^{n,\,high} = \frac{1}{2}\left(1 - \frac{\Delta t}{\Delta x}a(\rho_{i+\frac{1}{2}}^n)(q_{i+1}^n - q_i^n)\right) + \frac{1}{2}\left(1 + \frac{\Delta t}{\Delta x}a(\rho_{i-\frac{1}{2}}^n)(q_i^n - q_{i-1}^n)\right),$$

giving us the final forms

$$q_{i+\frac{1}{2}}^{n,\,high} = \frac{1 - \frac{\Delta t}{\Delta x}a(\rho_{i+\frac{1}{2}}^n)}{2}(q_{i+1}^n - q_i^n) \tag{4.23}$$

$$q_{i-\frac{1}{2}}^{n,\,high} = -\frac{1 + \frac{\Delta t}{\Delta x}a(\rho_{i-\frac{1}{2}}^n)}{2}(q_i^n - q_{i-1}^n). \tag{4.24}$$

Although this is a fairly involved numerical procedure it has very nice properties including stability, no limitations on data type, and it is TVD. We do a few simulations with this model and compare the results to our microscopic traffic model, (2.2).

4.3.3 Results of Comparison

Before we begin simulating the LWR model with the numerical method described above, we discuss what we hope to achieve from this. It is well documented in the literature that the LWR model does not predict the formation of stop and go waves, and overall does a pretty rough job of predicting certain traffic phenomena. We also know that the LWR model is TVD, implying that if initially traffic density is somewhat uniformly distributed, or close to a constant density, then it must retain, or decrease, its current amount of variance. This is something which we know is not always the case in traffic. Our microscopic model is built around the idea that these jams can form, and that they can severely disrupt the flow of traffic. The fact that these jams can form from nearly constant density implies a model having the TVD property cannot predict the formation of the types of jams studied in [12]. Therefore, an accurate traffic model should not possess this property. One might ask why we are bothering with these comparisons if the LWR is known to be inaccurate? Despite the models shortcomings, it has some very important strengths making it widely used. First and foremost, the model and its principles are conceptually easy to grasp. This allows the model to be used by anyone who a has basic understanding of partial-differential equations. This is not the case for higher order models. Another strength of this model is a basic numerical scheme can be implemented, and computed, with reasonable results in a short amount of time. Essentially, the model is convenient to use and believed to be good enough to get some reasonable results. With these ideas in mind we will not be using the LWR model as a benchmark to test our model; instead, we use our model to test the inaccuracies of the LWR model. This limits the comparisons to be done at speeds where our model is validated, therefore, we will make comparisons at speeds around $30\,km/h$. Since we expect the LWR to show significantly different dynamics than our microscopic model, we will also make comparisons based on predicted travel times around the circle. Microscopically, this will be done by average vehicle speeds around the track, and macroscopically, this will be done by averaging all speeds dictated by the fundamental diagram at each grid point.

We will run a total of 6 simulations, one low density test and one high density test for three different fundamental diagrams. Two of the three are the fundamental diagrams seen in Figure 4.2, and the third fundamental diagram is the one derived by our car interaction model, seen in Figure 4.6. The simulations will be run on a one kilometer

long track with a speed limit of $30\,km/h$.

We start with a plot of the two initial conditions used in these simulation. The first set of simulations will use the lower density initial condition seen on the left of Figure 4.12, and the second set will use the higher density initial condition seen on the right of Figure 4.12.

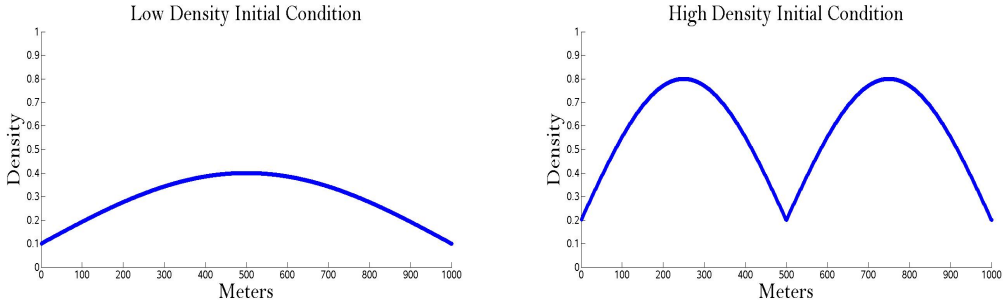

Figure 4.12: Initial conditions for Microscopic vs. Macroscopic comparisons.

The results from the low density comparison are shown in Figure 4.13. There is a lot of information shown here, so before we discuss the results we will clarify what is being displayed. Each of the six individual plots contains an image of the individual cars on the left, an estimation of the microscopic density in the middle, and finally the LWR model on the right. The microscopic model is dictating the behaviour of the cars shown on the left, and an approximate density at each time step is plotted in the middle. The two plots along the top have the LWR model using the Greenshields-like fundamental diagram, the middle two plots are using the hyperbolic tangent fundamental diagram, and the bottom row is using our derived fundamental diagram. The left column is showing the traffic conditions after approximately 5 seconds, and the right column shows conditions after approximately 40 seconds. The estimated time for a car to travel around the circle in the microscopic model is shown in the microscopic density plot, and the LWR model's travel time prediction is shown in the LWR plot.

We begin discussing the results of the first set of simulations by focusing on the plots down the left column of Figure 4.13. If we look at the shape of the curves we see that the Greenshields-like model, on the top, is closest to the shape possessed by our microscopic density. The microscopic model shows the minimal steepening to the left of the density peak, and minor flattening to the right of the density peak, but not to the same degree as shown by the other two fundamental diagrams. We see for all

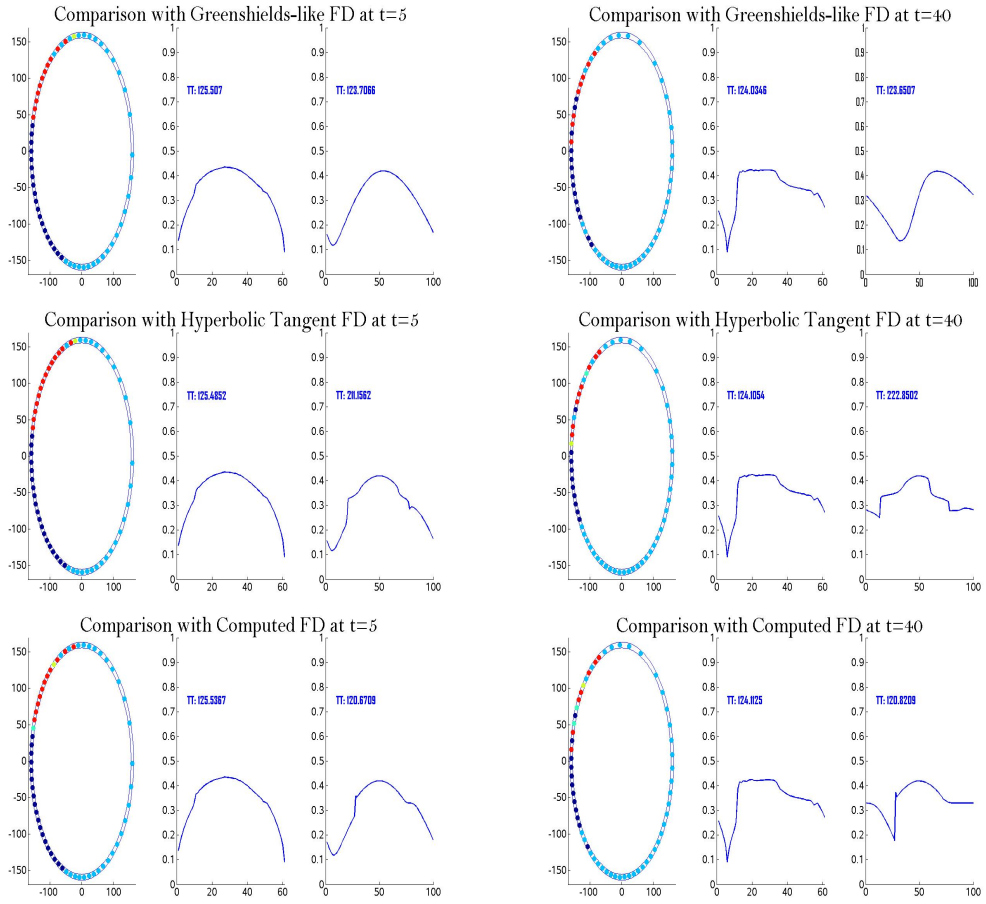

Figure 4.13: Microscopic vs. Macroscopic comparison for low density traffic.

fundamental diagrams that the LWR model predicts a shift to the right in density, which is not shown by the microscopic density. We ignore this for now because it is a minor inconsistency between the individual cars and the microscopic density. Looking at projected travel times around the 1 kilometer track, the Greenshields-like model is closest by estimating 123.7 seconds compared to the microscopic estimation of 125.5 seconds. The next closest is our derived fundamental diagram with an estimation of 120.6 seconds, and a distant third goes to the hyperbolic tangent with a terrible estimation of 211.1 seconds. The hyperbolic tangent predicts a long travel time because its flux drops to almost zero past densities of approximately 0.3. This is very different from what our microscopic model predicts. We now shift focus to the second plots which are approximately 40 seconds into the simulation. Looking only at the density distributions, we see that our computed fundamental diagram, (on the

bottom), gives the best approximation of the microscopic density. The Greenshields-like model is too smooth, and seems to have overestimated the total flux resulting in the density moving too far to the right. The hyperbolic tangent, (in the middle), looks to be the worst of the three due to the severe lack in flux in the higher densities. In terms of travel times, again the Greenshields-like is closest with an estimated 123.6 seconds compared to the microscopic estimation of approximately 124.0 seconds. The second best goes the our fundamental diagram with an estimation of 120.8, and the worst again goes to the hyperbolic tangent with an estimated travel time of 222.8 seconds. Overall, the Greenshields-like fundamental diagram performs best with accurate travel time estimations, and decent density approximations. The second best is our fundamental diagram with the hyperbolic tangent being a distant third. As we move to the higher density simulations we see a shift in which fundamental diagram performs best, we begin our analysis of these results.

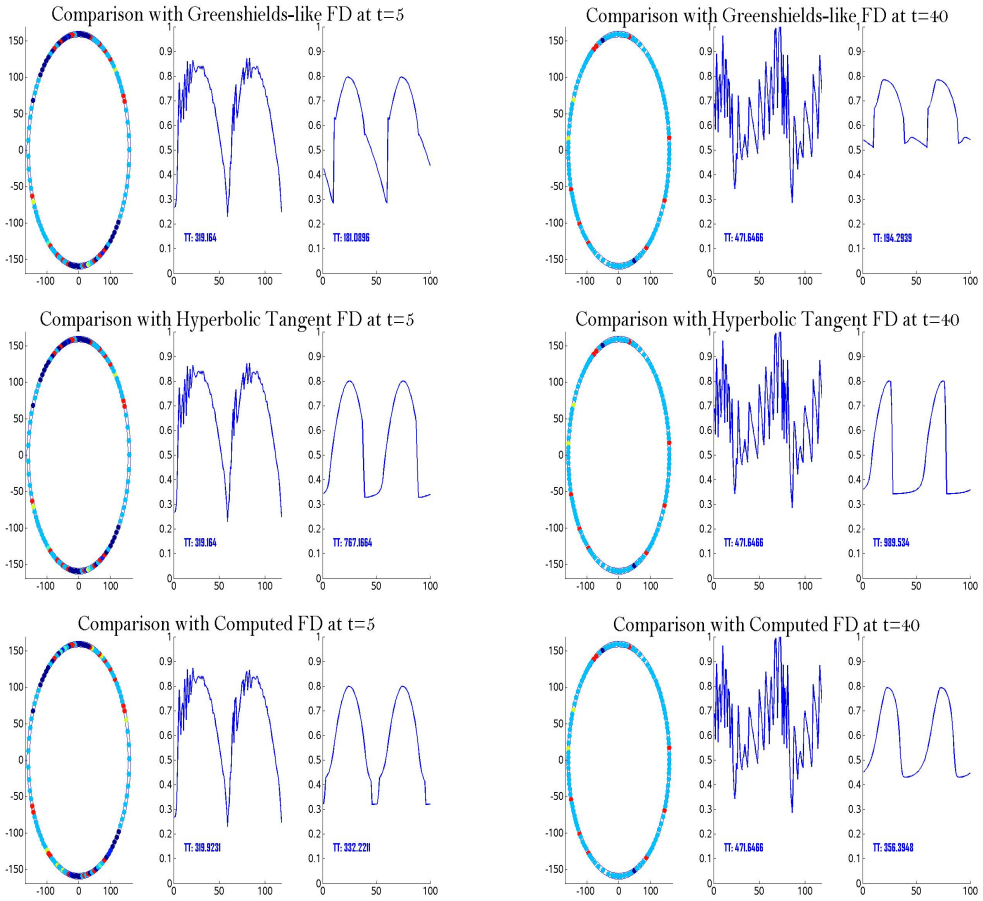

Figure 4.14: Microscopic vs. Macroscopic comparison for high density traffic.

The plots in Figure 4.14 have the same set up as in the previous set, with the Greenshields-like fundamental diagram on top, the hyperbolic tangent in the middle and our derived fundamental diagram on the bottom. Looking down the left column, results from early in the simulation, we see that the LWR model, for all three fundamental diagrams, fails to capture the initial formation of jams. From the outset we knew it was not possible for the LWR model to predict such behaviour due to the TVD property. Despite the missing detail, the density distributions of both the hyperbolic tangent and our fundamental diagram do a decent job of matching the microscopic density early in the simulation. At this point, the microscopic model predicts a travel time of approximately 319 seconds, with the next closest being our fundamental diagram predicting 332 seconds. The next closest is the Greenshields-like fundamental diagram with a prediction of 181 seconds, and the hyperbolic tangent predicts 767 seconds. We observe that the Greenshields-like fundamental diagram overestimates the flux, and that the hyperbolic tangent continues to significantly underestimate the flux at medium to high density. Looking at the second set of plots, we begin to see the extreme difference between the microscopic and macroscopic traffic predictions. If we ignore the oscillations in the microscopic density, we see there is still a presence of the original two peaks of density. Again, we have the hyperbolic tangent and our fundamental diagram doing a better job of matching these underlying peaks shown in the microscopic density. The large differences between microscopic and macroscopic predictions is not only visible in distribution of density, but also the predicted travel times. The microscopic model predicts a travel time of roughly 471 seconds, with the closest again being our fundamental diagram predicting 356 seconds. The Greenshields-like fundamental diagram predicts a 194 second travel time and the hyperbolic tangent predicted 989 seconds.

Chapter 5

Concluding Remarks and Outlook

We have designed a microscopic traffic model (2.2) to be used in the simulation and testing of small scale problems in traffic. The model was validated by recreating the experiment done in [12] and showing that it predicted nearly identical dynamics as seen in the experiment. The next step was the design and analysis of different intersection types. Our models of these intersections include some simplifying assumptions, for example, the exclusion of left turns. Many other details can be added to these models, including: Multiple lanes, cyclists and pedestrians, and adding more driver psychology into the merging process. For example, merging vehicles don't always wait until a car has exited the roundabout before feeling it is safe to merge, instead, they respond to cues from the exiting driver. Some cues a merging driver would look for are: Whether or not the potentially exiting vehicle has its blinker on, or, if this vehicle is showing signs of slowing down. Another assumption our model makes is that all drivers are exactly the same. This assumption has the advantage of driver consistency between tests, however, including different types of drivers is an important step in the complete analysis of an intersection's effectiveness. The car interaction model can easily account for this simply by individualizing the model parameters to each car and making them random variables. Not only can such details be added to the model itself, they can also be added to our analysis of these models. For example, the impact of hybrid cars in our fuel consumption analysis could be considered.

Using (2.2), we made comparisons between these two intersection types with many of the results confirming our intuition. For example, in the low density simulations we saw that fuel efficiency and flux results significantly favoured roundabouts over traffic lights. This agrees with expectations that cars having to stop and wait at red lights,

in low density, is a waste of fuel and inefficient in terms of flux. Of course, on our roadways this issue has been somewhat addressed through the use of sensors at traffic lights. Another example of these results matching our intuition, is the superiority of traffic lights when traffic is flowing with high flux, or at a medium density. When traffic is flowing at this high rate, traffic lights do an excellent job of retaining that high flow rate through the intersection, especially with long light cycles. In contrast, roundabouts force cars to slow down and merge, reducing the overall flux.

We also set out to make comparisons between our microscopic model and macroscopic models. Using (2.2), and the circular track used in the model calibration, we computed a fundamental diagram. Not only was the resulting fundamental diagram consistent with observations, but the process also reflected positively on some features of our model. One outcome was the presence of significant scattering in the unstable region of traffic and another was that our model predicts different fundamental diagrams depending on the speed limit. A simple calculation confirms that our fundamental diagram, computed for slow moving traffic, will not simply transfer over to highway traffic. This could potentially complicate things when trying to model a multi-lane highway with large differences in speeds from lane to lane.

The pursuit of a fuel consumption fundamental diagram has left some interesting and potentially useful questions to be answered. We first note that, as with the usual fundamental diagram, this fundamental diagram would have to be speed limit dependent. For simplicity we define FD_{fuel} to denote the fuel consumption fundamental diagram. Testing FD_{fuel}'s accuracy would not be very difficult, one could run a microscopic simulation with a fuel consumption model attached, and then translate the car positions into a density at each time step. At each step FD_{fuel} translates the density, ρ, into an estimated fuel consumption rate at that point $FD_{fuel}(\rho(x))$. The total fuel consumption rate over the road would be evaluated as $\int FD_{fuel}(\rho(x)) \cdot \rho(x)dx$.

The direct comparisons between our microscopic model and the LWR model proved to be quite useful. First, using our technique for comparing the two models, we were able to conclude that the LWR model performed best while using our computed fundamental diagram. More importantly, we showed this model's inability to capture any of the jams, or stop-and-go wave formation shown by our microscopic model. This leads to very inaccurate predictions of travel times around the track, and a poor estimation of the distribution of density. It also leads us to the conclusion that any total variation diminishing traffic model will not be able to produce all types of dynamics shown by our microscopic model.

Throughout this paper we have discussed several applications of a high accuracy microscopic traffic model. Through the use of our model, we have made progress in understanding which intersection types will best suit a given traffic scenario. Computation of a fundamental diagram allowed us to quantify the impact jam formation has on flux and fuel consumption, emphasizing the importance to avoid traffic congestion. Allowing our roads to become congested not only increases fuel consumption, but reduces flux causing the congestion to worsen. These results showcase the importance of collaboration between traffic modelers and traffic engineers.

Bibliography

[1] A. Aw and M. Rascle, Resurection of "second order" models of traffic flow. *SIAM J. Appl. Math.*, **60(3)**, (2000), 916–938.

[2] H. M. Zhang, A non-equilibrium trac model devoid of gas-like behaviour, *Trans. Research B*, **36** (2002), 275–290.

[3] M. Lighthill and G. Whitham, On kinetic waves II: A theory of traffic flow along crowded roads, *Proc. R. Soc. Lond. Ser. A Math. Phys. Eng. Sci.*, **229** (1956), 317–345.

[4] P. Richards, Shock waves on the highway, *Math. Models Public Syst.*, **1** (1971), 51–56.

[5] L.A. Richards, On Operational Analysis of Traffic Dynamics, *Journal of Applied Physics.*, **24(3)** (1953), 274–81.

[6] J.S. Tyler, The Characteristics of Model Following Systems as Synthesizes by Optimal Control, *IEEE Trans. Automatic Control.*, **AC-9** (1964), 485–98.

[7] G.O. Burnham and J. Seo and G.A. Bekey, Identification of human driver models in car following, *IEEE Trans. Automatic Control.*, **AC-19** (1974), 911–15.

[8] M. Herty and R. Illner, On stop-and-go waves in dense traffic. *Kinetic and Related Models.*, **1**, (2008), 437–452.

[9] M. Herty and R. Illner, Coupling of non-local driving behvaviour with fundamental diagrams. *Kinetic and Related Models.*, **5**, (2012), pp. 846.

[10] K. Nagel and M. Schreckenberg, A cellular automatan model for freeway traffic. *Journal de Physique I France.*, **2**, (1992), 2221–2229.

[11] B. Kerner and B. Kerner,A microscopic model for phase transitions in traffic flow. *J. Phys. A: Math. Gen.*, **35**, (2002), L31–L43.

[12] Y. Sugiyama et al., Traffic jams without bottlenecks-experimental evidence for the physical mechanism of the formation of a jam. *New Journal of Physics.*, **10**, (2008), 033001.

[13] K. Ahn, Microscopic fuel consumption and emission modeling. *Masters Thesis.*, (1998).